Lithos 155 (2012) 392–409

Contents lists available at SciVerse ScienceDirect

Lithos

journal homepage: www.elsevier.com/locate/lithos

The 3.1 Ga Nuggihalli chromite deposits, Western Dharwar craton (India): Geochemical and isotopic constraints on mantle sources, crustal evolution and implications for supercontinent formation and ore mineralization

Ria Mukherjee [a], Sisir K. Mondal [a,b,*], Robert Frei [c,e], Minik T. Rosing [d,e], Tod E. Waight [c], Hong Zhong [f], G.R. Ravindra Kumar [g]

[a] Department of Geological Sciences, Jadavpur University, Calcutta, India
[b] Department of Earth and Planetary Sciences, American Museum of Natural History, New York, USA
[c] Institute for Geography and Geology, University of Copenhagen, Denmark
[d] Natural History Museum of Denmark, University of Copenhagen, Denmark
[e] Nordic Center for Earth Evolution, Copenhagen, Denmark
[f] State Key Laboratory of Ore Deposit Geochemistry, Chinese Academy of Sciences, Guiyang, China
[g] Centre for Earth Science Studies, Trivandrum, India

ARTICLE INFO

Article history:
Received 16 July 2012
Accepted 1 October 2012
Available online 12 October 2012

Keywords:
Chromite
Komatiite
Magmatic fractionation
Supercontinent
Nuggihalli
Dharwar craton

ABSTRACT

Nuggihalli greenstone belt is one of the oldest greenstone belts (3.4–3.0 Ga) in the Western Dharwar craton, southern India. It consists of conformable metavolcanic (e.g., komatiite and komatiitic basalt) and metasedimentary rocks belonging to the Sargur Group. Sill-like ultramafic–mafic plutonic bodies are present within these schistose rocks which are in turn enclosed by tonalite–trondhjemite–granodiorite gneisses (TTG). The plutonic suite occurs as a layered succession of serpentinite (after dunite) and tremolite–chlorite–actinolite schist (after peridotite) hosting chromitite bodies, anorthosite, pyroxenite, and gabbro hosting magnetite bands. Whole-rock Sm–Nd data for the peridotite–anorthosite–pyroxenite–gabbro unit yield a correlation line with a slope corresponding to an age of 3125 ± 120 Ma (MSWD = 1.3) which is similar to ages of komatiitic rocks of the older greenstone belts in the craton. A whole rock Pb–Pb errorchron age of 2801 ± 110 Ma (MSWD = 102) has been obtained for the entire plutonic ultramafic–mafic suite; this represents (partial) redistribution/resetting of the U–Pb system during a younger metamorphic event and by the magmatic activity during formation of the younger greenstone belts. The positive ε_{Nd} values (+1.7 to +3.4) of the ultramafic–mafic rocks, and low initial $^{87}Sr/^{86}Sr$ values (at 3.1 Ga) of the gabbros (0.70097–0.70111) implies derivation of the parental magma from a depleted mantle source. The REE pattern of the metavolcanic schists bears resemblance with the pattern of Al-depleted komatiites. Major and trace element variation in the schists correspond with the fractionation trend exhibited by komatiites to komatiitic basalts in the older greenstone belts within the craton. Coherent patterns of whole-rock major and trace element data, along with the layered nature of the sill-like ultramafic–mafic rocks indicate that the plutonic and volcanic suites are related by analogous fractional crystallization processes. Comparison of our age data with global plutonic and volcanic ultramafic–mafic rock occurrences in greenstone belts supports an increase in komatiitic activity from 3.5 Ga to 2.7 Ga, which is most likely related to a supercontinent cycle. High-Mg magmas such as komatiites and their plutonic equivalents host important metal deposits like chromite, Ni-sulfide and minor PGE mineralization. The uneven distribution of metal deposits over time can be explained by supercontinent cycles. The 3.1 Ga chromite deposits of the Nuggihalli greenstone belt are perhaps related to the amalgamation stage of a supercontinent.

1. Introduction

Archean greenstone belts represent the site of continental crustal growth in the early Earth. The greenstone belts are composed of interlayered volcanic–sedimentary rocks that are surrounded by the tonalite–trondhjemite–granodiorite (TTG) gneisses (DeWit and Ashwal, 1995). Sill-like bodies of ultramafic and mafic rocks comprise an important component of greenstone belts, as for example in the Shurugwi greenstone belt (Zimbabwe craton; Stowe, 1987), Sukinda–Nuasahi–Jojohatu complexes in the Tomka–Daitari–Jamda–Koira greenstone belts (Singhbhum craton, eastern India; Mondal, 2009; Mondal et al., 2006), Nuggihalli–Holenarsipur–Krishnarajpet–Banasandra–Kalyadi greenstone belts (Western Dharwar craton, southern India; Mukherjee et al., 2010), Barberton greenstone

* Corresponding author at: Department of Geological Sciences, Jadavpur University, 188 Raja S.C. Mullik Road, Calcutta, 700032, India. Tel.: +91 33 24572730.
E-mail addresses: sisir.mondal@gmail.com, smondal@amnh.org (S.K. Mondal).

0024-4937/$ – see front matter © 2012 Elsevier B.V. All rights reserved.
http://dx.doi.org/10.1016/j.lithos.2012.10.001

belt (Jamestown Igneous complex, Kaapvaal craton, South Africa; DeWit et al., 1987), the Bird River sill within the Bird River greenstone belt (Superior craton, Canada; Mungall and Staff, 2008; Ohnenstetter et al., 1986), and the Obanga greenstone belt (Superior craton, Canada; Tomlinson et al., 2002). These ultramafic–mafic bodies are genetically related to high-Mg magmas such as komatiite, boninite or high-Mg siliceous basalt (Mondal, 2000; Mondal et al., 2006, 2007; Prendergast, 2008; Rollinson, 1997).

The relationship of the sill-like plutonic ultramafic–mafic rocks with the associated volcanics remains ambiguous. They have been considered to represent sill-like intrusions (Mondal et al., 2006; Prendergast, 2008), or these were originally sub-volcanic sill-like feeders to the overlying volcanic rocks that were tectonically emplaced alongside the volcanics during later deformation events (e.g., Lesher and Groves, 1986; Naldrett and Turner, 1977). Alternatively, they are also considered as the lower cumulate portion of thick komatiitic extrusions (Barnes et al., 1988; Donaldson et al., 1986; Hill et al., 1995). Resolving these questions requires precise geochronological data.

The main objective of our current research is to determine the age of the chromitite-bearing sill-like layered cumulates from the Nuggihalli greenstone belt, Western Dharwar craton, southern India (Fig. 1a). The sill-like layered unit comprises serpentinites (after dunite) and tremolite–chlorite–actinolite schists (after peridotite) that host chromitite bodies, anorthosites, pyroxenites, and gabbros that contain magnetite bodies. The plutonic suite is surrounded by the metavolcanic schistose unit of the older greenstone belts (supracrustals of the Sargur Group), which consists of the oldest rocks (3.4–3.0 Ga; Jayananda et al., 2008; Maya et al., 2011; Nutman et al., 1992; Ramakrishnan et al., 1994) reported from the Western Dharwar craton. Recent research by Mukherjee et al. (2010) has shown that the chromitite-bearing ultramafic–mafic plutonic suite was derived from high-Mg komatiitic basalt magma within an Archean suprasubduction zone setting.

In this study we present the first whole-rock Sm–Nd, Pb–Pb, and Rb–Sr isotope studies, and major and trace element geochemistry of the sill-like plutonic ultramafic–mafic rocks and associated schistose metavolcanic rocks from the Nuggihalli greenstone belt. Geochronological study of these rocks is significant as they are integral in defining the lithospheric evolution, and formation and stabilization of the Western Dharwar craton. Major and trace element geochemistry has been utilized to distinguish magmatic fractionation processes from the effects of alteration, metamorphism, and crustal contamination in the rocks, and also to determine the nature of the parental magma and mantle source. Integrated trace element and isotope geochemistry helps to elucidate the relationship between the plutonic ultramafic–mafic suite and the metavolcanic schistose unit in the Nuggihalli greenstone belt, as their contact relations have been obliterated in the field.

2. Geological background

The Nuggihalli greenstone belt is situated in the Western Dharwar craton in southern India (Fig. 1a). A 500 km long, N–S trending intrusive body of Closepet Granite (2.5 Ga; Taylor et al., 1988) has sub–divided the craton into a western and an eastern component (Fig. 1a). The Western Dharwar craton comprises older Archean supracrustal rocks that constitute the Sargur Group (Swami Nath and Ramakrishnan, 1981). The Sargur Group consists of sediments and igneous rocks that were metamorphosed to greenschist and amphibolite facies. The meta-igneous lithologies occur as both intrusive and volcanic ultramafic–mafic rocks with a compositional range from komatiite to komatiitic basalts and tholeiites (Ramakrishnan et al., 1994). The ultramafic–

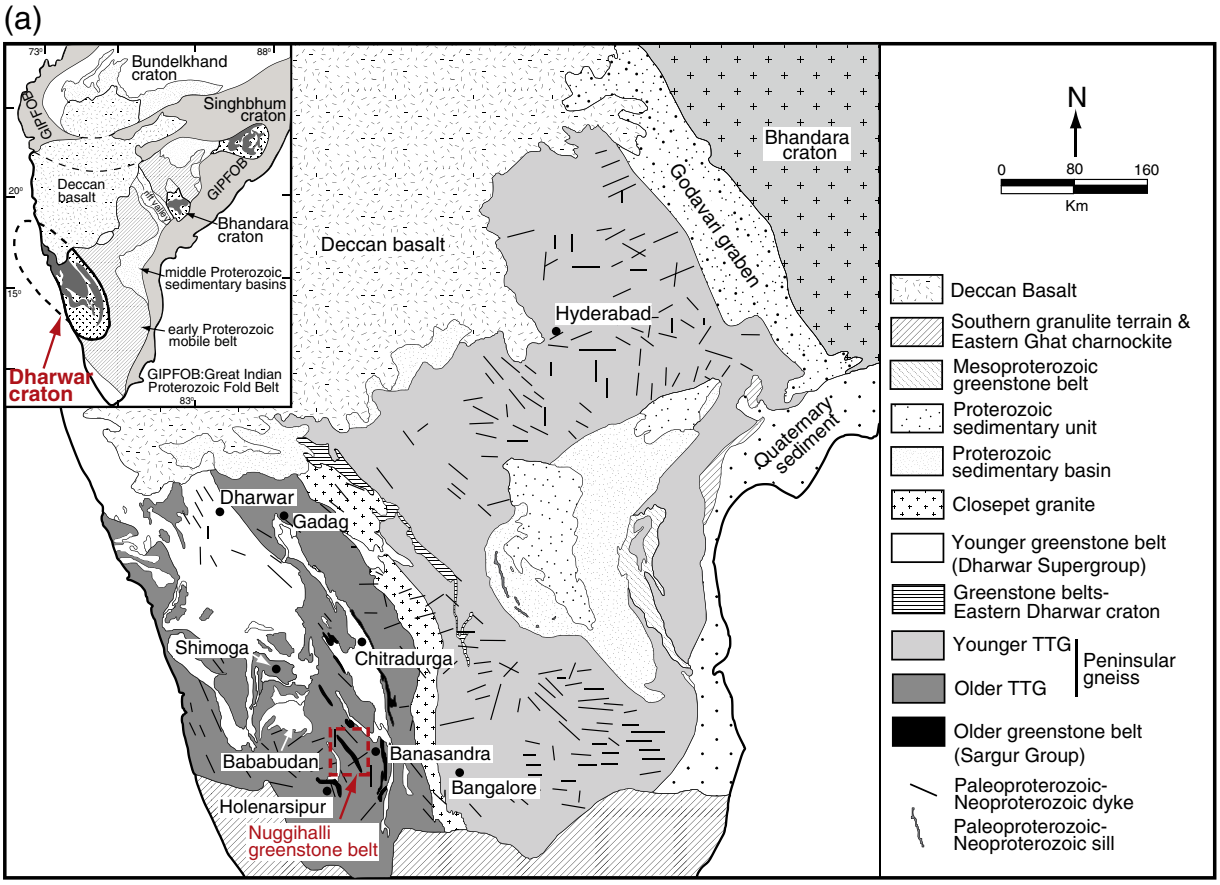

Fig. 1. (a) Generalized geology of the Dharwar craton showing location of the Nuggihalli greenstone belt (after Murthy, 1987; cited in Devaraju et al., 2009). Inset map portrays the generalized geology of the Indian shield showing Dharwar craton (compiled by Mondal et al., 2006; after Leelananadam et al., 2006; Radhakrishna and Naqvi, 1986). (b) Geology of the Nuggihalli greenstone belt showing locations of the chromite mining districts (after Jafri et al., 1983; cited in Devaraju et al., 2009). Sample locations are marked.

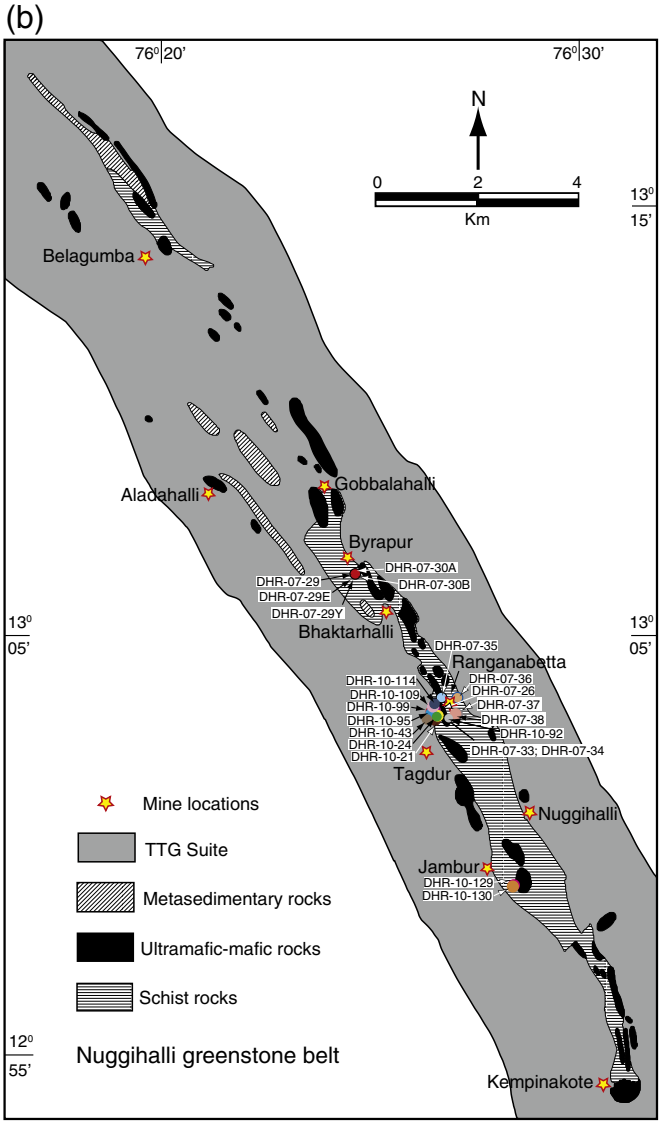

Fig. 1 (*continued*).

mafic rocks occur as linear belts, and are associated with clastic sediments (mainly quartzites) and banded iron formations, as found in the greenstone belts of Nuggihalli, Holenarsipur, Krishnarajpet, and Nagamangala. Rocks of the Sargur Group are unconformably overlain (Swami Nath and Ramakrishnan, 1981) by the younger supracrustals of the Dharwar Supergroup (younger greenstone belts ≈2.9–2.6 Ga; Taylor et al., 1984). The Dharwar Supergroup overlies the tonalite–trondhjemite–granodiorite (TTG) suite that acts as their basement, and is later intruded by the Closepet Granite at about 2.5 Ga.

The Nuggihalli greenstone belt is a linear belt (≈length 60 km; width ≈2 km) with a strong NNW–SSE trend (Fig. 1b). It consists of several *en echelon*, lenticular, dismembered, sill-like ultramafic–mafic bodies that are well exposed in the Tagdur mining district (Fig. 1b). The sill-like bodies are composed of layers of dunite (now serpentinite), peridotite (now tremolite–chlorite–actinolite schist), pyroxenite and gabbro. The sequence commences with a serpentinite and tremolite–chlorite–actinolite schist unit that hosts the chromitite ore bodies (≈50–500 m length; width ≈15 m). The chromitites appear as sigmoidal, lenticular, pod-shaped, and folded bodies (≈0.5 m length; width ≈0.3 m), with a nearly vertical dip (75°– 80°) and a range in strike from NW–SE to N–S with dip towards the east; at places they also have an E–W trend with dip towards the north. The serpentinite and peridotite are overlain by a pyroxenite unit, which is subsequently followed by a gabbro unit. The gabbro shows layering, and contains two conformable bands of titaniferous–vanadiferous magnetite at the base and top of the unit. The upper magnetite band has a N–S trend (width ≈1 m; Radhakrishnan et al., 1973), whereas the lower band (width ≈2 m) trends in the NNW–SSE direction; both dip towards the east.

The gabbro is overlain by an upper ultramafic unit of chromitite-bearing serpentinite. The chromitites (N–S trend, dipping west) in this unit are elongated, lenticular (length ≈100 m; width ≈15 m), and are more altered with a higher mode of carbonate (mainly magnesite; Table 1). The upper ultramafic unit is overlain by the schists that are variably altered, and possess a strong deformational fabric which imparts a lens-shaped geometry to the rocks. A lens-shaped E–W trending anorthosite unit (width ≈130 m) is observed in the Jambur mine (Fig. 1b), where it is interlayered with serpentinite. Overall, the rocks in the Nuggihalli greenstone belt are deformed and altered, with the deformation and alteration being linked to later metamorphism and secondary low temperature hydrothermal processes during serpentinization.

3. Samples and petrologic background

Samples have been collected from all the different lithological units across the entire stratigraphy of the Nuggihalli greenstone belt. The samples were collected from different mine sections and from outcrops. Most of the samples have been collected from the Tagdur mine, and also from the Byrapur and Bhaktarhalli mines of the greenstone belt (Fig. 1b). A detailed description of the samples is presented in Table 1 which is available online. The serpentinites are highly schistose and deformed rocks that are completely altered to an assemblage of antigorite, chlorite and magnesite. The upper serpentinite (DHR-07-36) that occurs above the gabbro shows a higher mode of magnesite (≈35% modal) relative to the other serpentinite samples. Chromites occur as an accessory phase (<2% modal) that are highly altered and compositionally zoned with ferritchromite rims and modified cores (Mukherjee et al., 2010). The chromitites are predominantly composed of coarse to medium-grained, euhedral, and polygonal chromite grains. Based on the modal proportions of the intercumulus silicates the chromitites can be identified as massive chromitite to net-textured, spotted- and schlieren-banded varieties (e.g., Mondal et al., 2006; Mukherjee et al., 2010). The intercumulus silicate minerals have been altered to antigorite, chlorite and minor carbonate. The peridotites are medium to fine grained, schistose, and composed of actinolite and chlorite grains with minor tremolite and talc. Fine-grained irregular shaped accessory chromite grains occur in the rock.

The anorthosites are coarse grained and consist of plagioclase, actinolite, chlorite and minor oxide minerals. The rock exhibits cumulate texture, where coarse and rounded plagioclase grains constitute the cumulus phase that are surrounded by the intercumulus actinolite and chlorite grains. The pyroxenite is a dark green rock that shares conformable contact with the lower magnetite band within the subsequent gabbro unit. The rock is altered and dominated by secondary minerals such as actinolite, chlorite and quartz; some hypersthene grains are also present. Disseminated oxides in the rock are ilmenite with exsolved patches of hematite. The gabbro is coarse-grained and ranges from melanocratic to slightly leucocratic, due to an increase in the abundance of plagioclase in the upper part of the unit. The rock retains the original cumulus texture; however, it is metamorphosed in most places with the development of quartz, chlorite and amphibole, along with magnetite and coarse- to medium-grained ilmenite.

The schists are mainly comprised of metagabbro, amphibolite schist, chlorite–quartz–actinolite schist and talc–chlorite schist. The metagabbro shows a well developed fabric and is composed of coarse-grained plagioclase and actinolite, along with chlorite, quartz and minor epidote. The schistose metagabbro differs from the previously discussed cumulate metagabbro in that it is more deformed, contains less plagioclase, and does not host magnetite bands. The quartz–chlorite–amphibole schist exhibits a weak fabric and is

Table 2
Major element on anhydrous basis (wt.%) and trace element (ppm) data of the samples from Nuggihalli greenstone belt.

	DHR-07-29 chromitite	DHR-07-29E chromitite	DHR-07-29Y chromitite	DHR-07-30A serpentinite[a]	DHR-07-30B serpentinite[a]	DHR-07-BH-1 serpentinite
SiO_2				39.20	39.48	
Al_2O_3				2.36	1.63	
TiO_2				0.14	0.10	
Fe_2O_3				10.58	10.09	
MnO				0.12	0.10	
MgO				47.12	47.80	
CaO				0.47	0.79	
Na_2O				0.01	0.01	
K_2O				0.01	0.01	
P_2O_5				0.02	0.02	
LOI				13.5	13.35	
Sc	0.06	0.28	1.55	1.01	18.43	6.06
Ti	57.80	61.52	170.9	49.55	6882	232.8
V	10.29	12.30	37.48	14.21	236.2	75.84
Cr	6497	8213	18095	4337	436.6	9654
Mn	268.7	342.5	647.4	271.8	1349	393.3
Co	22.78	25.43	62.25	23.33	77.27	71.37
Ni	1026	956.2	2506	1372	244.6	555.4
Cu	1.80	0.40	2.46	1.08	23.78	0.27
Zn	14.31	17.28	37.03	9.81	67.80	30.22
Ga	1.79	2.11	3.29	1.42	14.27	4.08
Rb	0.05	0.05	0.20	0.13	1.23	0.10
Sr	0.01	0.14	0.04	0.12	74.70	0.12
Y	0.29	0.06	0.12	0.08	8.39	0.08
Zr	1.29	1.31	1.87	8.77	76.17	0.68
Nb	0.17	0.15	0.51	0.19	5.20	0.34
Cs	–	0.01	0.03	0.01	0.04	0.01
Ba	–	0.01	0.05	0.21	6.34	0.22
Hf	0.04	0.04	0.05	0.21	2.09	0.02
Ta	0.25	0.18	0.69	0.24	0.71	0.72
Pb	0.25	0.69	0.88	0.39	3.48	0.09
Th	0.01	–	0.01	0.01	0.47	0.02
U	–	–	0.02	0.01	0.14	0.01
Mo	0.04	0.07	0.15	0.02	0.26	0.02
La	0.02	0.01	0.04	0.03	3.70	0.02
Ce	0.06	0.03	0.13	0.10	15.10	0.05
Pr	0.01	–	0.02	0.01	1.32	0.01
Nd	0.04	0.02	0.07	0.06	5.97	0.04
Sm	0.02	0.01	0.03	0.02	1.89	0.01
Eu	–	–	–	–	0.71	–
Gd	0.02	0.01	0.04	0.02	2.14	0.02
Tb	–	–	–	–	0.35	–
Dy	0.02	0.01	0.04	0.02	2.02	0.02
Ho	–	–	0.01	0.01	0.38	–
Er	0.02	0.01	0.03	0.02	0.99	0.01
Tm	–	–	–	–	0.13	–
Yb	0.01	0.01	0.02	0.02	0.77	0.02
Lu	–	–	–	–	0.11	–

	DHR-07-21 serpentinite[a]	DHR-07-24 serpentinite[a]	DHR-07-TD-6 serpentinite	DHR-07-36 serpentinite[a]	DHR-10-92 peridotite[b]	DHR-10-95 peridotite[b]
SiO_2	46.61	42.70		21.48	45.65	46.17
Al_2O_3	4.41	3.40		5.27	6.28	8.82
TiO_2	0.05	0.07		0.02	0.18	0.27
Fe_2O_3	10.21	10.63		11.53	11.24	11.07
MnO	0.09	0.16		0.33	0.07	0.09
MgO	37.35	39.52		61.23	30.21	22.96
CaO	1.28	3.51		0.13	6.36	9.65
Na_2O	0.01	0.01		0.02	0.01	0.94
K_2O	0.01	0.01		0.02	–	0.03
P_2O_5	0.01	0.01		0.01	–	–
LOI	11.00	16.90		33.60	4.71	3.03
Sc	3.92	3.75	1.04	1.13	8.20	7.42
Ti	268.6	381.7	638.5	68.32	701.0	1024
V	67.88	43.28	24.31	17.99	96.15	126.6
Cr	6690	2261	644.5	8130	3105	1750
Mn	556.1	724.1	628.4	1164	787.7	733.0
Co	99.01	104.3	90.50	31.74	60.59	47.85
Ni	1119	1415	2233	1273	387.7	427.0
Cu	0.18	24.42	0.69	1.44	77.20	11.30
Zn	24.57	18.18	20.92	12.98	12.97	10.22
Ga	3.37	2.54	1.32	4.08	3.91	4.63
Rb	0.29	0.03	0.02	0.26	0.01	0.03

(continued on next page)

Table 2 (*continued*)

	DHR-07-21 serpentinite[a]	DHR-07-24 serpentinite[a]	DHR-07-TD-6 serpentinite	DHR-07-36 serpentinite[a]	DHR-10-92 peridotite[b]	DHR-10-95 peridotite[b]
Sr	0.18	1.66	0.76	0.08	0.51	4.25
Y	0.28	0.36	0.49	0.13	1.18	1.55
Zr	1.94	0.15	6.64	0.31	4.26	3.30
Nb	0.26	0.32	1.44	0.05	0.19	0.17
Cs	0.01	0.01	0.04	0.01	-	-
Ba	0.05	0.10	0.01	0.02	0.18	0.59
Hf	0.06	0.01	0.21	0.01	0.14	0.19
Ta	0.46	0.45	0.86	0.10	0.24	0.20
Pb	0.01	0.05	0.19	0.36	0.004	–
Th	0.01	0.01	0.02	–	0.01	0.01
U	0.01	0.02	0.03	–	0.01	–
Mo	0.01	0.19	0.14	0.02	0.02	0.06
La	0.09	0.03	0.35	0.02	0.03	0.06
Ce	0.14	0.13	1.46	0.06	0.17	0.41
Pr	0.03	0.02	0.21	0.01	0.03	0.07
Nd	0.10	0.09	1.08	0.05	0.20	0.45
Sm	0.03	0.05	0.25	0.02	0.10	0.18
Eu	0.01	–	0.05	–	0.02	0.10
Gd	0.03	0.06	0.25	0.02	0.15	0.27
Tb	0.01	0.01	0.04	–	0.03	0.05
Dy	0.05	0.08	0.21	0.02	0.24	0.35
Ho	0.01	0.02	0.04	0.01	0.06	0.08
Er	0.04	0.07	0.12	0.02	0.18	0.22
Tm	0.01	0.01	0.01	–	0.03	0.03
Yb	0.06	0.08	0.09	0.03	0.19	0.23
Lu	0.01	0.01	0.01	–	0.03	0.03

	DHR-10-99 peridotite[b]	DHR-10-129 anorthosite[b]	DHR-10-130 anorthosite[b]	DHR-07-26 pyroxenite[a]	DHR-07-35 gabbro[a]	DHR-10-43 gabbro[b]
SiO_2	42.34	45.59	45.48	53.83	50.22	47.33
Al_2O_3	8.10	28.57	29.63	8.69	17.87	12.70
TiO_2	0.16	0.14	0.13	0.91	2.28	1.40
Fe_2O_3	10.60	3.40	3.17	15.94	11.77	15.83
MnO	0.12	0.03	0.02	0.18	0.17	0.14
MgO	31.08	3.64	3.30	10.46	4.25	8.41
CaO	7.59	16.39	16.27	8.88	10.69	13.03
Na_2O	0.02	2.17	1.93	0.87	2.60	1.03
K_2O	–	0.06	0.05	0.13	0.11	0.08
P_2O_5	–	0.01	0.01	0.11	0.06	0.04
LOI	4.44	0.43	0.63	2.4	1.43	2.07
Sc	6.27	2.62	5.53	9.07	20.60	19.95
Ti	614.9	610.2	598.6	4518	10829	8002
V	77.19	62.05	61.67	126.9	108.1	531.0
Cr	2491	172.7	201.7	726.8	5.37	147.0
Mn	872.8	226.6	124.0	1408	1174	967.6
Co	61.39	11.71	10.91	70.90	43.61	44.58
Ni	365.3	23.19	21.87	404.1	1.79	56.13
Cu	3.15	5.57	1.70	178.5	6.36	236.9
Zn	13.76	8.04	6.90	86.12	55.68	72.69
Ga	4.06	12.82	12.76	9.75	18.72	16.42
Rb	0.01	0.03	0.01	0.13	0.07	0.02
Sr	0.58	50.26	24.01	7.98	126.0	131.8
Y	1.29	0.44	0.11	3.74	4.69	3.58
Zr	3.78	1.70	1.09	51.76	12.77	4.02
Nb	0.21	0.28	0.23	10.15	1.87	0.72
Cs	–	–	–	–	–	–
Ba	0.35	0.61	1.02	5.77	7.72	3.10
Hf	0.13	0.08	0.06	1.39	0.40	0.25
Ta	0.24	0.12	0.14	0.99	0.44	0.29
Pb	0.04	0.43	0.35	0.22	0.46	0.32
Th	0.01	0.04	–	0.24	0.02	0.02
U	0.01	0.02	0.01	0.10	0.07	0.03
Mo	0.03	0.17	0.57	0.07	0.20	0.24
La	0.06	0.16	0.05	4.23	1.29	0.80
Ce	0.25	0.74	0.09	9.43	3.17	1.73
Pr	0.06	0.04	0.01	1.21	0.56	0.35
Nd	0.35	0.18	0.07	4.81	2.94	1.91
Sm	0.14	0.05	0.02	1.13	0.90	0.66
Eu	0.05	0.03	0.01	0.38	0.53	0.34
Gd	0.20	0.07	0.03	1.13	1.05	0.84
Tb	0.04	0.01	0.01	0.18	0.17	0.14
Dy	0.29	0.08	0.05	0.99	1.06	0.94
Ho	0.07	0.02	0.01	0.18	0.22	0.20
Er	0.21	0.05	0.04	0.50	0.62	0.54
Tm	0.04	0.01	0.01	0.07	0.09	0.07

Table 2 (*continued*)

	DHR-10-99 peridotite[b]	DHR-10-129 anorthosite[b]	DHR-10-130 anorthosite[b]	DHR-07-26 pyroxenite[a]	DHR-07-35 gabbro[a]	DHR-10-43 gabbro[b]
Yb	0.23	0.05	0.05	0.41	0.50	0.44
Lu	0.03	0.01	0.01	0.06	0.08	0.06

	DHR-10-109 gabbro[b]	DHR-10-114 gabbro[b]	DHR-07-33 metagabbro[a]	DHR-07-34 chl-qtz-act schist[a]	DHR-07-37 talc-chlorite schist[a]	DHR-07-38 amphibolite schist[a]
SiO_2	37.98	48.21	53.03	48.99	53.88	53.77
Al_2O_3	17.27	14.13	11.35	15.31	6.88	14.69
TiO_2	1.57	1.04	1.19	1.06	0.14	2.01
Fe_2O_3	20.88	15.03	13.27	13.76	8.49	10.56
MnO	0.14	0.21	0.19	0.20	0.10	0.13
MgO	10.82	8.44	8.78	7.78	28.13	5.96
CaO	9.10	11.16	8.74	9.48	2.34	9.20
Na_2O	2.11	1.57	3.14	3.00	0.02	2.89
K_2O	0.09	0.12	0.21	0.35	0.01	0.23
P_2O_5	0.03	0.08	0.10	0.08	0.02	0.57
LOI	2.74	2.06	1.11	1.79	6.47	1.17
Sc	4.71	13.74	17.66	21.81	4.32	11.21
Ti	8922	6226	6971	6137	537.5	11896
V	739.0	279.4	239.9	292.8	84.52	312.2
Cr	76.99	318.5	430.6	242.6	2323	100.2
Mn	892.1	1405	1345	1476	660.9	991.9
Co	73.89	48.83	75.45	51.60	80.26	46.16
Ni	232.7	138.1	237.0	128.9	1262	70.29
Cu	492.9	100.4	23.17	91.86	40.21	51.41
Zn	89.29	82.57	66.59	70.76	62.44	84.87
Ga	18.92	15.61	13.73	16.72	3.94	20.71
Rb	0.05	0.03	1.16	0.67	0.04	0.15
Sr	92.67	32.98	69.26	88.73	0.53	58.86
Y	1.29	4.98	7.58	7.65	0.29	20.77
Zr	3.30	18.92	69.62	11.89	1.78	139.8
Nb	0.71	2.65	4.66	2.78	0.15	11.94
Cs	–	–	0.04	0.01	–	–
Ba	7.08	9.57	5.57	8.72	0.03	15.60
Hf	0.15	0.61	1.91	0.44	0.07	3.21
Ta	1.96	0.22	0.47	0.42	0.06	0.69
Pb	0.20	0.30	3.22	5.71	0.12	2.02
Th	0.02	0.04	0.42	0.07	–	0.36
U	0.04	0.07	0.13	0.08	0.01	0.45
Mo	0.12	0.19	0.22	0.14	0.06	0.39
La	0.84	1.73	3.35	1.67	0.02	7.32
Ce	1.95	3.13	13.71	4.44	0.08	17.85
Pr	0.28	0.66	1.19	0.69	0.01	2.79
Nd	1.38	3.40	5.29	3.53	0.06	12.59
Sm	0.36	0.94	1.67	1.15	0.03	3.54
Eu	0.26	0.35	0.63	0.45	0.01	1.18
Gd	0.39	1.14	1.93	1.50	0.03	4.00
Tb	0.06	0.18	0.31	0.27	0.01	0.70
Dy	0.37	1.10	1.85	1.72	0.06	4.41
Ho	0.07	0.23	0.34	0.37	0.01	0.95
Er	0.20	0.63	0.90	1.08	0.05	2.75
Tm	0.03	0.08	0.12	0.15	0.01	0.37
Yb	0.16	0.52	0.72	0.94	0.05	2.30
Lu	0.02	0.07	0.09	0.13	0.01	0.33

Major element data from a: ALS Laboratory (Guangzhou, China) b: major CESS (India); data of all trace elements from GEUS (Copenhagen, Denmark); LOI values shown for information purpose.

composed of actinolite along with chlorite, recrystallized quartz grains, minor plagioclase (altered to epidote), anhedral hematite and lath-shaped ilmenite that occur at the grain boundaries of the silicate minerals. The amphibolite schist is fine-grained, sheared and composed of actinolite, quartz, minor chlorite, plagioclase, hematite, and ilmenite. The talc–chlorite schist shows intense deformation in the form of crenulations and puckers; chevron folds are common. The rock is almost entirely composed of talc.

4. Analytical methods

The samples were pulverized in a tungsten carbide mortar at the Institute of Geology and Geography, University of Copenhagen for bulk rock major and trace element analyses. Major elements were determined on the PANalytical Axios-advance X-ray fluorescence spectrometer (XRF) at the ALS Laboratory (Guangzhou, China), using fused lithium–tetraborate glass pellets. The international standards SY-4 and STSD-4 were used for analytical quality control and the analytical precision is better than 5%. Major elements for some of the samples were analysed at the Centre for Earth Science Studies (Trivandrum, India), using a Bruker S4 Pioneer Wavelength Dispersive X-ray fluorescence (WD-XRF) spectrometer. Fused glass discs (30 mm) were used for analysis that were prepared following determination of loss on ignition, by fusing exactly 1 g of finely powdered sample mixed with 5 g of lithium tetra-metaborate flux, in a platinum crucible at 1100 °C using Claisse Fluxer. The standards used were ultramafic rock standards from the USGS, DTS1 and DTS2 and UB–N from CRPG (France). Detection limit of major element was ~0.01% and analytical precision is better than 1%. The major element oxides have been recalculated on an anhydrous basis and tabulated in Table 2. Totals of major element oxides are

100 ± 0.04 wt.%. Trace element concentrations on bulk solutions were analyzed by ICP-MS on the Perkin Elmer Elan 6100 DRC facility of the Geological Survey of Greenland and Denmark (GEUS). The standard BHVO-2 was used for trace element analysis. Appendices A, B, and C tabulate the standard, reference and duplicate data for both major and trace element analytical protocols, which are available online.

Bulk rock Nd–Pb–Sr isotopic analyses were performed by isotope dilution using TIMS at the Institute of Geography and Geology at the University of Copenhagen. For whole rock Sm–Nd and Sr isotopic analyses, 1 g of powdered rock sample was spiked with a mixed ^{147}Sm–^{150}Nd spike and dissolved in a mixture of concentrated HF and 14 N HNO_3 in Teflon beakers on a hot plate for 72 h. Chemical separation of Sr and REEs from whole rocks was carried out on conventional 12 ml glass stem cation exchange columns (Sr and total REE cuts), followed by a separation of Sm and Nd from total REEs using Tristchem/Eichrom™ Ln-resin charged in 4 ml pre-fabricated plastic columns (BioRad). Sr fractions stripped from the cation columns were subsequently cleaned from residual matrix elements by separation over 100 μl Tristchem/Eichrom™ SrSpec resin in disposable pipette-tip columns with a fitted frit according to a modified recipe published by Horowitz et al. (1992). Isotope analyses were carried out in multidynamic mode on the VG Sector 54-IT instrument. Nd ratios were normalized to $^{146}Nd/^{144}Nd = 0.7219$. The mean value of our long-term internal JM Nd reference solution analyses (referenced against the Geological Survey of Japan Shin Etsu Nd standard) is 0.51109 for $^{143}Nd/^{144}Nd$, with a 2σ external reproducibility of ± 0.000015 (fifty-five measurements). Sr isotopes were analysed in multidynamic mode using $^{86}Sr/^{88}Sr = 0.1194$ as the normalizing ratio for the correction for thermal fractionation. The mean $^{87}Sr/^{86}Sr$ value of the NIST 987 Sr standard measured during the analyses of the sample batch was 0.710242 ± 0.000016 ($n = 4$; 2σ).

For whole rock Pb isotope analysis powdered samples were dissolved by treating with concentrated HF-14N HNO_3 mix and finally by 9N HCl. A conventional HCl–HBr elution recipe was used for both the separation over 0.5 ml glass columns charged with AG–1 × 8 anion resins and the final purification of the Pb concentrates over 300 μl Teflon columns. Fractionation for Pb was controlled by repeat analyses of the NBS 981 standard and amounted to 0.103 ± 0.007%/a.m.u. (2σ; $n = 5$) relative to the values proposed by Todt et al. (1993).

5. Results

5.1. Geochemical variations

Given the altered nature of the rocks all the major elements show scatter with respect to MgO, however, some of the elements still provide information on magmatic conditions (Fig. 2). Al_2O_3 and TiO_2 exhibit a distinct negative relation with MgO except for some scattered values shown by the gabbros, metavolcanic schists and the pyroxenite (Fig. 2b, c). The elements Al and Ti are relatively immobile during metamorphism and secondary alteration (Kerrich et al., 1998; Pearce and Norry, 1979) hence they are successful in retaining the magmatic trend. The serpentinites show a contrasting positive relation of TiO_2 with MgO in Fig. 2b, which is due to alteration of accessory chromites to Ti-rich ferritchromite and the presence of secondary magnetite in these rocks (Mukherjee et al., 2010). The rest of the major elements SiO_2, CaO, and the alkali elements ($Na_2O + K_2O$) show large scatter with MgO, but a negative trend is discernable (Fig. 2a, d, e). P_2O_5 shows a positive variation with TiO_2 (Fig. 2f); the gabbros plot slightly away from the trend due to their higher TiO_2 contents. A positive correlation is also seen in the Ni and Cr versus MgO diagrams (Fig. 2g, i); the serpentinites however show scattered Cr values which is expected due to the intense alteration of the accessory chromite grains in these rocks to ferritchromite and magnetite. An overall negative relation is observed when Ni and Cr are plotted against TiO_2 (Fig. 2h, j), where the latter is taken to be an index of fractionation. Among the metavolcanic schists one sample show consistently low values for the major and trace elements, the concentrations of which matches with the range shown by the serpentinites and peridotites of the plutonic suite (Fig. 2). In Fig. 2, the major and trace element concentrations of the Nuggihalli rocks have been compared with a typical Al-depleted komatiite and komatiitic basalt from the Barberton greenstone belt (Kaapvaal craton; Arndt et al., 2008), and an Al-undepleted komatiite and komatiitic basalt from the Abitibi greenstone belt (Superior craton; Fan and Kerrich, 1997). Komatiitic rocks of the Sargur group reported by Jayananda et al. (2008) from the Western Dharwar craton have also been included for comparison.

The chondrite-normalized REE patterns of the Nuggihalli rocks have been plotted in Fig. 3 and compared with komatiites from the Western Dharwar craton, and the Al–depleted and undepleted komatiite and komatiitic basalts from the Barberton and Abitibi greenstone belts respectively. The chondrite-normalized REE patterns of the chromitites, serpentinites, peridotites, and anorthosites are flat (Fig. 3a), and the rocks contain low abundances of REE. The chromitites show strong negative Eu anomalies (Eu anomaly ≈ 0.22–0.37) similar to the serpentinites (Eu anomaly ≈ 0.22–0.63), which is an outcome of hydrothermal alteration as explained by Sun and Nesbitt (1978) and Arndt et al. (1989) for hydrothermally altered komatiites and basalts within Archean greenstone belts. The peridotites either show a slightly positive Eu anomaly (≈ 1.34) or a negative anomaly (≈ 0.54), while the anorthosites show distinct positive Eu anomaly (≈ 1.42–1.58) (Fig. 3a). The positive Eu anomaly is due to the presence of plagioclase in these rocks.

The pyroxenite and gabbro displays superchondritic REE abundances relative to the ultramafic plutonic rocks (Fig. 3b). The gabbros exhibit positive Eu anomalies (Eu anomaly ≈ 1.03–2.12) due to the presence of plagioclase feldspar, except for sample DHR-10-114. Other than sample DHR-07-37 (talc–chlorite schist), the metavolcanic schists have superchondritic REE abundances with flat chondritic REE patterns. Sample DHR-07-37 (talc–chlorite schist) shows subchondritic REE abundances and LREE depleted pattern ($La_N/Sm_N \approx 0.52$; Fig. 3c). The metagabbro (DHR-07-33) shows HREE depleted character similar to the cumulate gabbro of the plutonic suite ($Gd_N/Yb_N \approx 2.18$; Fig. 3c). The REE pattern of sample DHR-07-38 show almost flat REEs with slight HREE depletion ($Gd_N/Yb_N \approx 1.41$).

In the chondrite-normalized multi-element plot (Fig. 3d, e), the ultramafic–mafic plutonic rocks show parallel patterns, where they are characterized by strong enrichment in Ti (≈ 0.1–25 × chondrite), depletion in Rb (0.003–0.05 × chondrite), and moderate enrichment in Sr (0.1–18 × chondrite), U (0.4–13 × chondrite) and Th (0.1–8 × chondrite); positive anomaly of Rb is observed for the serpentinites DHR-07-36, DHR-07-21, and the chromitites (Fig. 3d). A distinctly positive Zr–Hf anomaly is exhibited by few of the serpentinites, chromitites, and a peridotite; remainder of the samples show low Zr/Hf ratios except for the pyroxenite (Fig. 3e). Compared to the serpentinites and peridotites, the gabbros and pyroxenite display relatively higher concentration of the trace elements (Fig. 3e). The metavolcanic schists are characterized by similar trace element patterns as observed in the plutonic rocks (Fig. 3e). The talc–chlorite schist (DHR-07-37) shows strongest Ti anomaly (1.2 × chondrite) among the schistose samples.

5.2. Geochronology

The whole-rock Sm–Nd data of the ultramafic–mafic rocks from the plutonic suite, namely the peridotite–anorthosite–pyroxenite–gabbro unit from the Nuggihalli greenstone belt, define a nine point isochron corresponding to an age of 3125 ± 120 Ma (MSWD = 1.3; $^{143}Nd/^{144}Nd$ initial = 0.50872 ± 0.00015), and an ε_{Nd} value of + 2.8 (Fig. 4a). A considerable variation in the $^{147}Sm/^{144}Nd$ ratios of the ultramafic–mafic samples ensures a good spread of data points about the regression line in Fig. 4a. The ultramafic rocks such as serpentinite and chromitite, and the metavolcanic schists do not help to better constrain the isochron, and instead enhance the scatter about the correlation line. This

results from disturbances of the Sm–Nd isotope system in these rocks during secondary alteration (serpentinization) and metamorphism. The initial ε_{Nd} (3.1 Ga) values of the peridotites, anorthosites, pyroxenite and gabbros are uniformly positive, and vary from +1.7 to +3.8 (Table 3a). Such values are extremely variable for the schists and show a range from −3.7 to +7, again reflecting a severe post-formational disturbance of the Sm-Nd system in these rocks.

A whole-rock Sm–Nd age for komatiitic rocks belonging to the older Sargur Group, from Nuggihalli and the surrounding stratigraphically equivalent greenstone belts of Ghattihosahalli, J.C. Pura, Banasandra and Kalyadi has been presented by Jayananda et al. (2008). They obtained a 16-point whole-rock Sm–Nd isochron age of 3352 ± 110 Ma ($^{143}Nd/^{144}Nd$ initial = 0.50838 ± 0.00015; ε_{Nd} +2.0 ± 3.0) as the age of komatiite eruption in the Western Dharwar craton, which is indistinguishable within errors from the age of the plutonic ultramafic–mafic suite reported herein. On comparing the whole-rock Sm–Nd data of the metavolcanic schists from our study with the isochron obtained by Jayananda et al. (2008) in Fig. 4b, it is observed that the schists do not lie on Jayananda et al's isochron which is due to variable hydrothermal alteration of the rocks.

The whole-rock Rb–Sr isotope data do not yield an isochron and suggest disturbances of the isotopic system, in particular due to the low concentrations of both Rb and Sr in some samples, which make them susceptible to perturbations (and analytical errors) (Table 3b). The initial $^{87}Sr/^{86}Sr$ ratios of the gabbros are very low and show a range from 0.70111 to 0.70286.

The bulk rock Pb isotope data obtained in our study are plotted in a conventional common-Pb isotope diagram (Fig. 5), that contains the two-stage evolution curve for average crustal Pb (Stacey and Kramers, 1975). The correlation lines are calculated and plotted using the program ISOPLOT for Excel by Ludwig (2008). In the $^{206/204}Pb$ versus $^{207/204}Pb$ diagram, all the plutonic ultramafic–mafic rocks, excluding the pyroxenite, are plotted together (Fig. 5). These rocks define a correlation line with a slope corresponding to an age of 2801 ± 110 Ma (Fig. 5). The large scatter of data points about the errorchron is reflected by the very high MSWD (mean squares of weighted deviates) value of 102, which

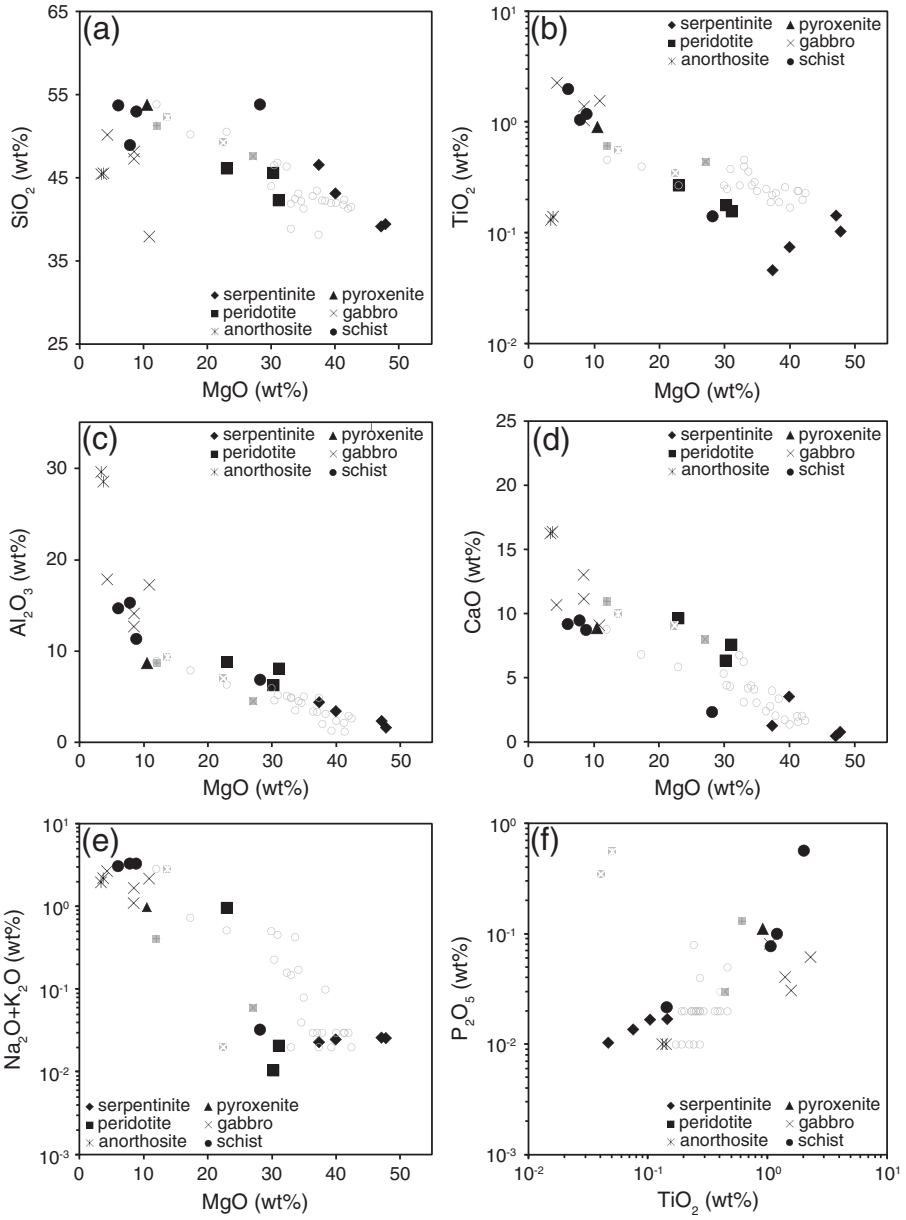

Fig. 2. Variation diagrams for selected major (anhydrous basis) and trace elements (a) MgO versus SiO_2 (b) MgO versus TiO_2 (c) MgO versus Al_2O_3 (d) MgO versus CaO (e) MgO versus $Na_2O + K_2O$ (f) TiO_2 versus P_2O_5 (g) MgO versus Ni (h) TiO_2 versus Ni (i) MgO versus Cr (j) TiO_2 versus Cr. ○ komatiite, WDC (Jayananda et al., 2008); ⊠ Barberton komatiite (Arndt et al., 2008); ▦ Barberton komatiite basalt (Arndt et al., 2008); ⊠ Abitibi komatiite (Fan and Kerrich, 1997); ▦ Abitibi komatiite basalt (Fan and Kerrich, 1997).

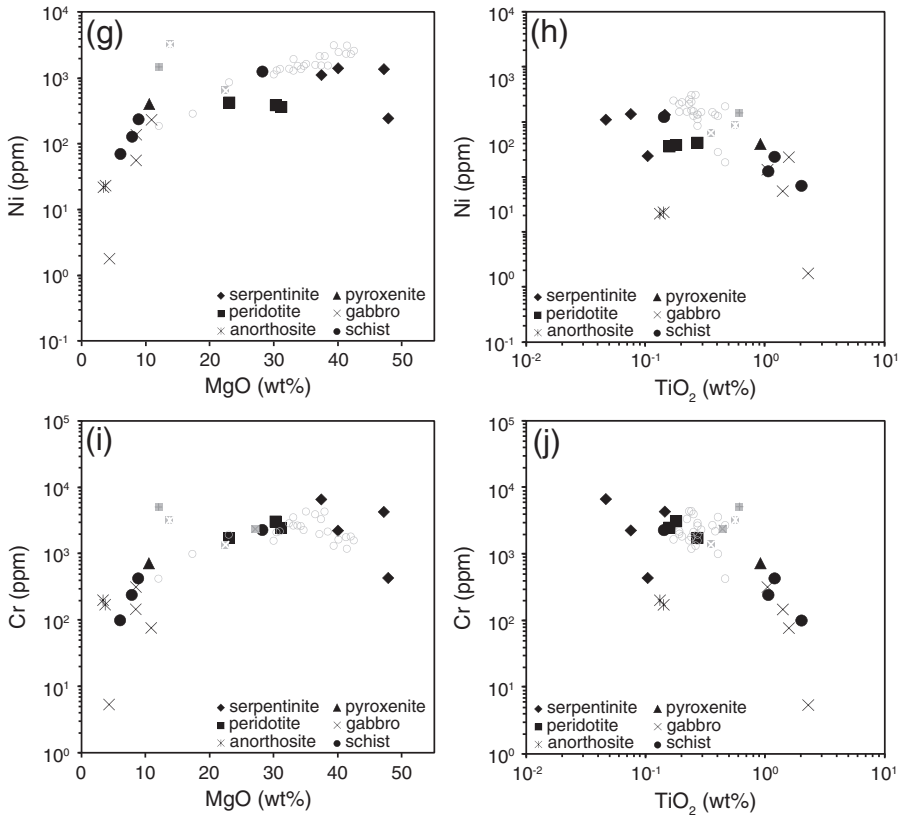

Fig. 2 (*continued*).

indicates scatter beyond analytical reasons, such as later disturbances in Pb isotopes during hydrothermal alteration or metamorphism. The pyroxenite sample is excluded from the regression calculation because of its very high radiogenic values of $^{206/204}$Pb (72.660), $^{207/204}$Pb (24.638) and $^{208/204}$Pb (123.527) (Table 3c). The reason for these radiogenic Pb isotope values are not understood, but we associate this signature with the likely presence of a U–Th-rich accessory mineral, potentially monazite, which was introduced during later hydrothermal alteration. The metavolcanic schists do not define a Pb–Pb isochron. The perturbations in Pb isotopes in these schists are understood from the very unradiogenic values (in relation to the antiquity of these rocks) of present day $^{206/204}$Pb, $^{207/204}$Pb, and $^{208/204}$Pb ratios (Table 3c), which indicate mobilization and loss of U and Th during secondary alteration processes. This is also reflected in the low μ values (6.82–7.75; Table 3c) of the chromitites, serpentinites, anorthosites, peridotites and a gabbro. In contrast, some very radiogenic Pb isotope ratios in rest of the samples imply the addition of U and Th during secondary enrichment events that led to their exceptionally high μ values of 8.34–13.66 (Table 3c).

6. Discussion

6.1. The 3.1 Ga age of the chromite deposits, crustal evolution and constraints on source mantle

Previous geochronological work in the Western Dharwar craton has mostly been conducted on the mafic and felsic rocks of the younger greenstone belts (i.e. the Dharwar Supergroup, Bhaskar Rao et al., 1992; Drury et al., 1983, 1987; Kumar et al., 1996; Peucat et al., 1995; Taylor et al., 1984), the surrounding TTG rocks (i.e. the Peninsular Gneiss and trondhjemite plutons, Beckinsale et al., 1980; Monrad, 1983; Stroh et al., 1983; Taylor et al., 1984; Meen et al., 1992), and on the late Archean granites (Bhaskar Rao et al., 1992; Meen et al., 1992; Taylor et al., 1988). Geochronological investigations of the Sargur Group of rocks (i.e. the older greenstone sequence) were conducted mainly in the Holenarsipur greenstone belt, in the Western Dharwar craton (Fig. 1a). Based on previous works, the Sargur Group were considered to be early Archean (>3.5 Ga) as they were intruded by the 3.4–3.3 Ga TTG rocks (Gorur Gneiss) near the Holenarsipur belt (Beckinsale et al., 1980, 1982). Others were of the opinion that the Sargur Group were middle Archean in age (≈3.2–3.0 Ga) because of the intrusion of 3.1–3.0 Ga TTG into the Sargur Group elsewhere in the Western Dharwar craton (e.g., Ramakrishnan et al., 1994). The age of deposition of the sedimentary protoliths belonging to the Sargur Group was considered to be between 3.1 and 3.0 Ga by Nutman et al. (1992) based on dating of detrital zircon grains in garnetiferous pelitic schists and quartzites (3.5–3.1 Ga and 3.2–3.1 Ga respectively), and the intrusions of TTG into these rocks (2.9–3.0 Ga). Similar interpretations were presented by Ramakrishnan et al. (1994) who considered a maximum age of the metasediments to be 3250±5 Ma based on the Pb–Pb zircon age of metaquartzites from the J.C. Pura belt, and Bidyananda et al. (2003) who obtained a 3.2 Ga U–Pb age of zircons from quartz–mica–chlorite schists in the Nuggihalli greenstone belt. Younger Pb ages of 2.96 Ga obtained in metamorphic zircons with low Th/U ratios (<0.05) (Nutman et al., 1992), and 2.9–2.7 Ga in rims of zoned zircon grains (Bidyananda et al., 2003) were considered by the authors to represent the age of later metamorphic imprints.

The metavolcanics of the older greenstone belts (i.e. the Sargur Group metavolcanics) were dated by Jayananda et al. (2008), where the timing of eruption of the komatiitic magma in the craton was constrained at 3352±110 Ma based on a whole-rock Sm–Nd isochron. The geochemistry of the komatiites indicated melting of a plume source at different depths. The associated tonalite–trondhjemite–granodiorite (TTG) gneisses were considered to have formed in an arc setting. A plume–arc interaction model was thus suggested to explain the spatial association of komatiites and the surrounding TTG in the craton.

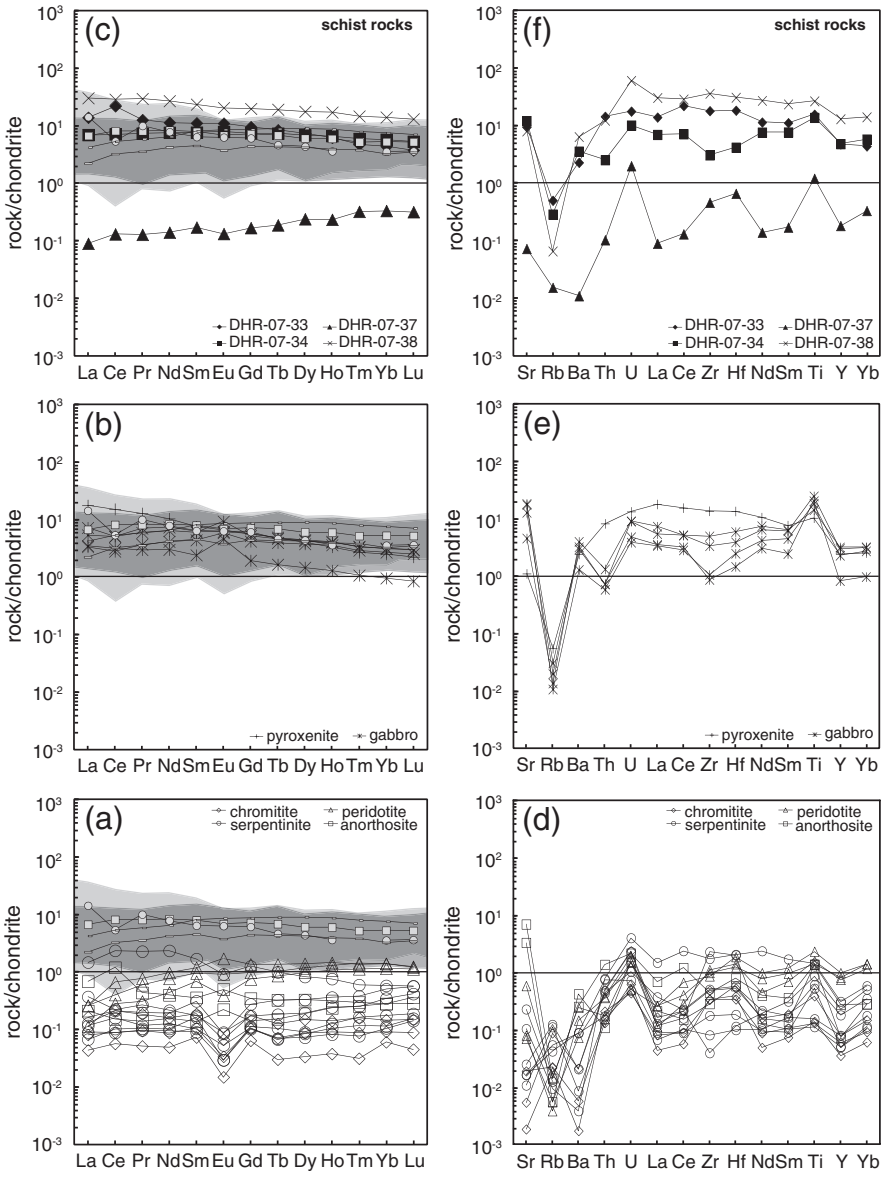

Fig. 3. Chondrite normalized REE diagrams of (a) chromitite, serpentinite, peridotite, and anorthosite (b) pyroxenite and gabbro and (c) schist rocks from the Nuggihalli greenstone belt. Chondrite normalized multi-element plot of (d) chromitite, serpentinite, peridotite, and anorthosite (e) pyroxenite and gabbro and (f) schist rocks. Normalised chondrite values from McDonough and Sun (1995). The field of Al–depleted komatiites (grey) and Al-undepleted komatiites (light grey) from the Western Dharwar craton (Jayananda et al., 2008) has been shaded. DHR-07-33: metagabbro; DHR-07-34: quartz–chlorite–amphibole schist; DHR-07-37: talc-chlorite schist; DHR-07-38: amphibolite schist; —□— Barberton komatiite (Arndt et al., 2008); —○— Barberton komatiitic basalt (Arndt et al., 2008); —— Abitibi komatiite (Fan and Kerrich, 1997); —— Abitibi komatiitic basalt (Fan and Kerrich, 1997).

Recently Maya et al. (2011) obtained a 3136 ± 200 Ma whole-rock Sm–Nd isochron for nine samples of komatiites from the Sargur equivalent Banasandra schist belt in the Western Dharwar craton (Fig. 1a). The komatiites yielded a positive ε_{Nd} (3.15 Ga) value of +3.5. Thus, the Sargur Group supracrustals formed in a protracted time period from 3.4 to 3.0 Ga, which is consistent with the observation that very short but distinct pulses of magmatism spanning up to 50 Ma generates the komatiitic–tholeiitic rock sequences in greenstone belts (e.g., Bryan and Ernst, 2008 and references therein). A simplified summary of the stratigraphy and crustal evolution of the Western Dharwar craton is presented in Table 4.

The first whole-rock Sm–Nd isochron age of 3125 ± 120 Ma for the chromitite-bearing sill-like ultramafic–mafic rocks, and their similarity within the limits of errors to the age of komatiites (Jayananda et al., 2008; Maya et al., 2011) in the older greenstone belts of the Western Dharwar craton, implies that plutonic magmatism occurred concomitantly with eruption of the komatiitic magma that are the protoliths to the schistose lithologies in the Nuggihalli and equivalent greenstone belts of the Western Dharwar craton. The average T_{DM} model age of DePaolo for the peridotite, anorthosite, pyroxenite and gabbro is 3.17 Ga. This implies that the parental magmas for the plutonic and volcanic ultramafic–mafic suites were rapidly emplaced in the crust (considering the error ranges for both plutonic and volcanic suites of the older greenstone belts).

The Pb–Pb age of 2801 ± 110 Ma, for the plutonic ultramafic–mafic rocks obtained in this study, is a metamorphic age that is inferred from the 2.9–2.7 Ga age of metamorphosed zircons in metasediments of the Sargur Group (Bidyananda et al., 2003; Nutman et al., 1992). The 2.8 Ga age is also close to the reported Sm–Nd ages of 2.85–2.75 Ga (Kumar et al., 1996) for mafic to felsic metavolcanic rocks of the younger supracrustals (Dharwar Supergroup) in the Bababudan and Chitradurga greenstone belts within the Western Dharwar craton. The Pb isotopes for the Nuggihalli ultramafic–mafic plutonic suite may have been reset to a younger age during emplacement of the igneous rocks of the younger greenstone belts, owing to loss of Pb from the minerals due to increased diffusion facilitated by the thermal effect.

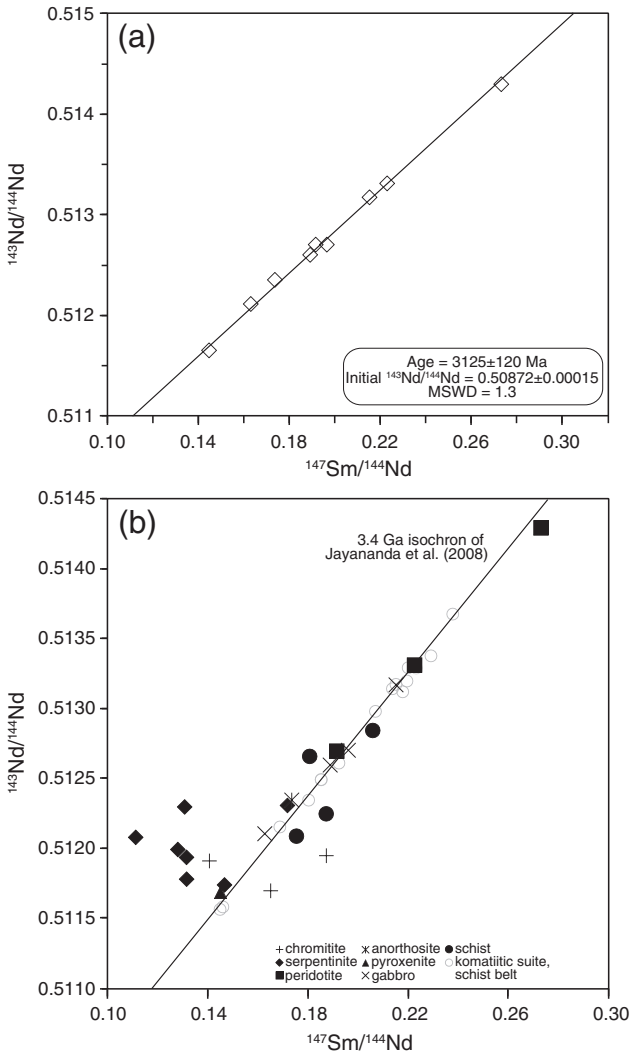

Fig. 4. (a) Whole-rock Sm–Nd isochron of peridotites–anorthosites–pyroxenite–gabbro. (b) Comparison of metavolcanic schist samples from the Nuggihalli greenstone belt with the 3.4 Ga Sm–Nd isochron of Jayananda et al. (2008) obtained from komatiites of the Sargur equivalent greenstone belts, Western Dharwar craton. DHR-07-33: metagabbro; DHR-07-34: quartz–chlorite–amphibole schist; DHR-07-37: talc–chlorite schist; DHR-07-38: amphibolite schist.

The ε_{Nd} values (at 3100 Ma) for the ultramafic–mafic rocks are mostly positive indicating a depleted mantle source for the Nuggihalli rocks (Table 3a). The ε_{Nd} value obtained for the whole-rock Sm–Nd isochron (3125 ± 120 Ma) is +2.8, and the average initial ε_{Nd} value of the peridotites, pyroxenite, anorthosites and gabbros is +2.72, which are slightly higher than the expected ε_{Nd} value of +2.0 for the depleted mantle at 3100 Ma (De Paolo, 1981). The schists, on the other hand, show variable ε_{Nd} values (at 3100 Ma) that average +0.44. Extremely negative and low positive values of ε_{Nd} (Table 3c) imply open-system processes during hydrothermal alteration and metamorphism which changed the pristine Sm/Nd ratios in these rocks at some later stage. Crustal contamination can also give rise to negative ε_{Nd} values, but this can be ruled out because trace element and REE composition of the Nuggihalli rocks do not support crustal contamination (Figs. 3, 6). Recently Dey (2012) has conducted an extensive review of ^{147}Sm–^{143}Nd isotopic data from ultramafic–mafic rocks, TTGs and granitoids of the Eastern and Western Dharwar craton. Though the ε_{Nd} values of the ultramafic–mafic volcanic rocks from the older greenstone belts of the Western Dharwar craton indicate a depleted mantle source, the mafic metavolcanics of the younger Dharwar Supergroup do not show any evidence of mantle source depletion, from which Dey (2012) surmised that mantle re-fertilization was a significant process that occurred in the Western Dharwar craton after formation of the older greenstone belts.

The Rb–Sr isotope data of the rocks from our study are highly variable and most of them are not considered to be representative of initial compositions (Table 3b). Nevertheless, the initial $^{87}Sr/^{86}Sr$ ratio (at 3100 Ma) of the gabbros (excluding DHR-10-114), which have relatively high Sr concentrations and low Rb/Sr ratios that minimize possible disturbances and errors during calculation of initial composition, may still be utilized to make inferences about the mantle source. The range of initial $^{87}Sr/^{86}Sr$ ratio in the gabbro (0.70097–0.70111) matches with the $^{87}Sr/^{86}Sr$ ratio of 0.7006 for the depleted mantle at 3100 Ma (Bell et al., 1982). In summary, the Nd and Sr isotope characteristics of some of the relatively less altered rocks from the Nuggihalli greenstone belt support the derivation of their parental magma from a depleted mantle source.

6.2. Magmatic fractionation

In Fig. 2, progressive enrichment is observed in the absolute concentrations of major and incompatible trace elements, from komatiites to komatiitic basalts in the Barberton and Abitibi greenstone belts (Arndt et al., 2008; Fan and Kerrich, 1997). Jayananda et al. (2008) have shown the occurrences of both komatiites and komatiitic basalts in the older greenstone belts of the Western Dharwar craton (e.g., J.C. Pura and Kalyadi belts), however, the composition of the komatiites reported by them are far too magnesian (≈33–42 wt.%) for a komatiitic flow (≈24–30 wt.%; Arndt et al., 2008); these are expected to represent olivine adcumulates that occur at the lower portion of thick komatiitic flows (e.g., Barnes, 2006; Hill et al., 1995). The basaltic komatiites were considered by Jayananda et al. (2008) to be co-magmatic with the komatiites from which they were derived by olivine and pyroxene fractionation. The variations in major and trace element concentrations of the metavolcanic schists from our study, correspond with such a variation exhibited by the komatiitic suite of the Western Dharwar craton (Fig. 2). The talc–chlorite schist (DHR-07-37) is observed to plot alongside the komatiites, while the other schist samples plot at the komatiitic basalt end in Fig. 2. Differentiation can occur within a thick volcanic komatiitic flow (Barnes, 2006; Hill et al., 1995), and in the Nuggihalli belt grain size variation has been observed within the schistose rocks. The major and trace element patterns of the ultramafic plutonic rocks and gabbro are also observed to be similar to the above differentiation trend (Fig. 2).

The REE patterns of the metavolcanic schists (except DHR-07-37) match with the pattern of Al-depleted komatiites of Jayananda et al. (2008), and with typical Al-depleted komatiites from the Barberton greenstone belt (Fig. 3c). Mukherjee et al. (2010) conducted a detailed study of unaltered chromites from the massive chromitites and computed their probable parental magma composition from the relation of Maurel and Maurel (1982), who showed that the Al_2O_3 (wt.%) in spinel is a function of Al_2O_3 (wt.%) in the melt. Kamenetsky et al. (2001) showed from melt inclusion data within chromite from volcanic rocks, that a linear relationship exists between the Al_2O_3 and TiO_2 content in chromite and the melt from which it crystallized. The calculated Al_2O_3, TiO_2 and FeO/MgO indicated that the parental melt of the Nuggihalli chromitite was a low–Al komatiitic basalt. The composition of the calculated parental melt, and the unaltered chromites from massive chromitite, plotted in the high-Ti arc field in the spinel Al_2O_3 versus TiO_2 tectonic discrimination diagram of Kamenetsky et al. (2001) (Fig. 8d of Mukherjee et al., 2010).

To further test whether fractional crystallization was responsible for generating the plutonic rock sequence observed in the Nuggihalli greenstone belt, we took the help of the MELTS algorithm of Ghiorso and Sack (1995). Al-depleted komatiite from the Western Dharwar craton (Jayananda et al., 2008) was taken to be the parental magma that was isobarically fractionated at 1638 °C and 2 Kbar pressure with the

Table 3a
Bulk rock Sm–Nd isotopic data of samples from the Nuggihalli greenstone belt, Western Dharwar craton.

Sample	Lithology	Sm (ppm)	Nd (ppm)	$^{147}Sm/^{144}Nd$	$^{143}Nd/^{144}Nd$	$\pm 2\sigma$	$(^{143}Nd/^{144}Nd)_i$ (3100 Ma)	T_{CHUR}	T_{DM} DePaolo	ε_{Nd} (3100 Ma)
DHR-07-29	chromitite	0.03	0.11	0.18719	0.511953	0.000044	0.508119			−9.63
DHR-07-29E	chromitite	0.04	0.15	0.16495	0.511702	0.000077	0.508324			−5.61
DHR-07-29Y	chromitite	0.04	0.16	0.14044	0.511916	0.000065	0.509039	1.95	2.58	8.45
DHR-07-30A	serpentinite	0.10	0.55	0.11100	0.512084	0.000055	0.509811	0.98	1.59	23.63
DHR-07-30B	serpentinite	0.11	0.53	0.12783	0.511997	0.000080	0.509380	1.42	2.05	15.14
DHR-07-BH-1	serpentinite	0.05	0.16	0.17165	0.512313	0.000016	0.508797	1.97	3.05	3.69
DHR-07-21	serpentinite	0.14	0.66	0.13130	0.511941	0.000018	0.509252	1.62	2.24	12.64
DHR-07-24	serpentinite	0.21	0.95	0.13056	0.512302	0.000023	0.509628	0.77	1.56	20.03
DHR-07-TD-6	serpentinite	0.84	3.45	0.14648	0.511744	0.000020	0.508744	2.70	3.20	2.64
DHR-07-36	serpentinite	0.30	1.36	0.13134	0.511785	0.000030	0.509095	1.98	2.54	9.55
DHR-10-92	peridotite	0.25	0.56	0.27299	0.514299	0.000017	0.508708	3.29	2.96	1.93
DHR-10-95	peridotite	0.55	1.50	0.22246	0.513317	0.000008	0.508761	3.98	2.92	2.98
DHR-10-99	peridotite	0.43	1.35	0.19136	0.512701	0.000024	0.508782		3.07	3.39
DHR-10-130	anorthosite	0.28	0.98	0.17336	0.512352	0.000025	0.508801	1.86	3.03	3.77
DHR-07-26	pyroxenite	2.16	9.04	0.14444	0.511653	0.000005	0.508695	2.85	3.31	1.68
DHR-07-35	gabbro	1.84	5.89	0.18873	0.512602	0.000004	0.508736	0.70	3.36	2.49
DHR-10-43	gabbro	1.19	3.34	0.21503	0.513176	0.000009	0.508771		2.93	3.19
DHR-10-109	gabbro	0.58	2.15	0.16257	0.512110	0.000007	0.508781	2.35	3.11	3.37
DHR-10-114	gabbro	2.38	7.36	0.19599	0.512707	0.000009	0.508693		3.82	1.65
DHR-07-33	schists	2.79	9.01	0.18713	0.512253	0.000005	0.508420			−3.72
DHR-07-34	schists	1.71	5.03	0.20573	0.512849	0.000007	0.508636	3.54		0.52
DHR-07-37	schists	0.16	0.54	0.18052	0.512664	0.000010	0.508967		2.24	7.03
DHR-07-38	schists	6.27	21.66	0.17523	0.512093	0.000005	0.508505	3.83		−2.06

fO_2 kept at QFM. The sequence of minerals that fractionated from this magma was olivine (1618 °C), olivine + chrome-spinel (1598 °C), orthopyroxene + chrome-spinel (1318 °C), pigeonite + chrome-spinel (1238 °C), pigeonite + augite + chrome-spinel (1218 °C), pigeonite + augite + feldspar + spinel (1197 °C), pigeonite + augite + feldspar + magnetite (1157 °C), augite + feldspar + magnetite (1078 °C). The composition of olivine obtained through MELTS is in the range of $Fo_{94.5–85.3}$, which matches with the range of olivine composition in dunites ($Fo_{95–91}$) within Archean greenstone belts (Barnes, 2006; Mondal et al., 2006), and with olivine compositions previously reported from serpentinised peridotites in the Nuggihalli greenstone belt ($Fo_{90–86}$; Bidyananda and Mitra, 2005). The orthopyroxene composition obtained through MELTS is enstatite (En 84% Fs 13% Wo 3%), and it matches with the range of orthopyroxene compositions within pyroxenites genetically linked to high-Mg parental magma (komatiite or boninite) in Archean greenstone belts. The common examples include orthopyroxene from the Nuasahi–Sukinda massifs, Singhbhum craton (En 86–92% Fs 7–10% Wo 0.7–4%; Mondal et al., 2006), and the Inyala chromite mines, Zimbabwe craton (En 88–89% Fs 11–12% Wo 0.2–0.5%; Rollinson, 1997). The initial composition of augite obtained through MELTS (En 53% Fs 15% Wo 32%), matched with the analysis of clinopyroxenes reported by Bidyananda and Mitra (2005) from serpentinised peridotites in Nuggihalli (En 56% Fs 13% Wo 32%). The initial feldspar composition varied from $An_{79.5–73}$ and matched with the range of An content in anorthosites of Archean greenstone belts ($An_{88–70}$; Ashwal, 1993). Thus an anorthosite body could be generated from this komatiitic magma. Continued fractionation changed the feldspar composition to An_{63}, where along with augite and accessory magnetite the gabbro could be formed (condition at 1078 °C).

In summary, the sequence of minerals obtained by the MELTS algorithm matched with the plutonic rock sequence in Nuggihalli where we have dunites, chromitites, peridotites, and anorthosites which are followed by gabbros with cumulus magnetite. A similar sequence of minerals was obtained by experimenting with a typical Al–depleted komatiite from the Barberton greenstone belt (Arndt et al., 2008), the only difference being that chrome–spinel was the first mineral to

Table 3b
Bulk rock Rb-Sr data of samples from the Nuggihalli greenstone belt, Western Dharwar craton.

Sample	Lithology	Rb (ppm)	Sr (ppm)	$^{87}Rb/^{86}Sr$	$^{86}Sr/^{87}Sr$	$\pm 2\sigma$	$(^{86}Sr/^{87}Sr)_i$ (3100 Ma)
DHR-07-29	chromitite	0.05	0.01	10.818	0.71324	0.00009	
DHR-07-29E	chromitite	0.05	0.14	1.085	0.71120	0.00002	
DHR-07-29Y	chromitite	0.20	0.04	14.763	0.71318	0.00003	
DHR-07-30A	serpentinite	0.13	0.12	3.002	0.71095	0.00012	
DHR-07-30B	serpentinite	1.23	74.70	0.048	0.71600	0.00005	0.71385
DHR-07-BH-1	serpentinite	0.10	0.12	2.372	0.71046	0.00003	
DHR-07-21	serpentinite	0.29	0.18	4.530	0.72800	0.00007	
DHR-07-24	serpentinite	0.03	1.66	0.050	0.70758	0.00005	0.70532
DHR-07-36	serpentinite	0.26	0.08	9.517	0.70589	0.00003	
DHR-10-92	peridotite	0.01	0.51	0.073	0.71111	0.00008	0.70781
DHR-10-95	peridotite	0.03	4.25	0.023	0.70577	0.00003	0.70472
DHR-10-99	peridotite	0.01	0.58	0.044	0.70485	0.00002	0.70287
DHR-10-129	anorthosite	0.03	50.26	0.002	0.70202	0.00003	0.70193
DHR-10-130	anorthosite	0.01	24.01	0.002	0.70250	0.00003	0.70243
DHR-07-26	pyroxenite	0.13	7.98	0.046	0.70648	0.00002	0.70442
DHR-07-35	gabbro	0.07	125.95	0.002	0.70104	0.00003	0.70096
DHR-10-43	gabbro	0.02	131.84	0.001	0.70113	0.00001	0.70111
DHR-10-109	gabbro	0.05	92.67	0.001	0.70117	0.00002	0.70111
DHR-10-114	gabbro	0.03	32.98	0.003	0.70298	0.00002	0.70286
DHR-07-33	schists	1.16	69.26	0.049	0.71144	0.00001	0.70926
DHR-07-34	schists	0.67	88.73	0.022	0.71810	0.00003	0.71711
DHR-07-37	schists	0.04	0.53	0.194	0.71313	0.00002	0.70440
DHR-07-38	schists	0.15	58.86	0.008	0.70335	0.00002	0.70301

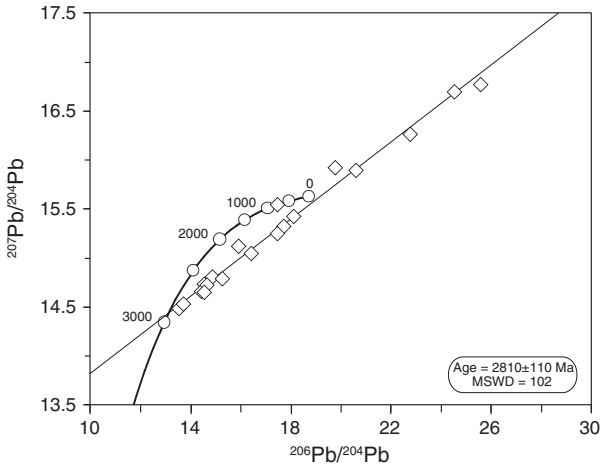

Fig. 5. Whole-rock $^{207}Pb/^{204}Pb$ versus $^{206}Pb/^{204}Pb$ isochron of chromitite, serpentinites and gabbro. The mantle curve was drawn assuming Stacey and Kramers (1975) two-stage model for Pb evolution.

appear on the liquidus rather than olivine, and the feldspar composition obtained was far too calcic ($An_{94.2}$). The An content obtained for the Barberton komatiite, matched with the An content ($An_{92–95}$) of anorthosites reported by Naqvi and Hussain (1979), from the stratigraphically equivalent Holenarsipur greenstone belt in the Western Dharwar craton.

Mungall and Staff (2008) had modeled the petrogenesis of chromitite bodies, within similar sill-like complexes in the Blackbird deposit, Superior craton, Canada using MELTS computational program. In this complex, the chromitite lenses are enclosed within deformed meta-dunite and meta-harzburgite bodies which are thoroughly altered to talc and carbonate. Mungall and Staff (2008) inferred that the chromitites formed from picritic magmas which assimilated water-rich iron formation. In the case of the Nuggihalli chromitite-bearing ultramafic–mafic rocks, the required sequence of minerals could not be modeled by fractionally crystallizing a picritic parental melt using MELTS. Application of the MELTS program with other parental melts like Archean boninites and high-Mg siliceous basalt did not produce the plutonic rock sequences of the Nuggihalli greenstone belt.

Crustal contamination of the parental komatiitic magma for the Nuggihalli rocks, can be firmly eliminated based on plots of the most incompatible elements versus immobile elements in Fig. 6. The potential contaminant of the parental komatiitic magma may be the surrounding TTG rocks, and therefore the average data of TTGs (3.3 Ga) from the Holenarsipur greenstone belt in the Western Dharwar craton has been plotted in this figure It is observed that the data of the Nuggihalli rocks (both plutonic and volcanic suites) plot away from the field of the TTGs, thus indicating that crustal contamination did not occur in the parental komatiitic magma. The scatter of samples in Fig. 6 is caused mainly by hydrothermal alteration and metamorphism. The komatiites and komatiitic basalts from the Western Dharwar craton (Jayananda et al., 2008) have been included in this figure for comparison, and they also do not show any evidence of crustal contamination (Fig. 6).

Though the field relationships between the sill-like ultramafic–mafic rock suite and the metavolcanics are not clear, the geochronology and geochemical data could be integrated to imply that the sill-like ultramafic–mafic rocks may be the plutonic equivalents of the metavolcanic schists that have now been tectonically juxtaposed with the plutonic ultramafic–mafic suite (e.g., Naldrett and Turner, 1977). The komatiitic protolith of the schists were contemporaneous with the plutonic suite and formed from similar parental magma. Parental magmas for both the suites experienced parallel fractionational crystallization from komatiite to a komatiitic basalt.

Jayananda et al. (2008) explained the close–spatial association of the TTGs and komatiites in the Western Dharwar craton to represent a plume–arc setting. The trace element patterns of TTGs characterized by low HREE (especially Y and Yb) and negative HFSE (e.g., Nb, Ta, Ti) anomalies, requires the melting of garnet and rutile bearing subducting eclogitic slab at depths in excess of 50–60 km in subduction zones (Moyen, 2011). Although many workers argue against the role of subduction and insist on TTG genesis by delamination of dense oceanic crust into the mantle, in which case the anhydrous melts generated do not represent tonalite composition (e.g., Moyen and Martin, 2012 and references therein). The most popular model for genesis of komatiites is by mantle plumes arising from the core–mantle boundary that represents anomalously high mantle temperatures and anhydrous conditions (Arndt et al., 2008; Campbell et al., 1989; Fan and Kerrich, 1997; Herzberg, 1995). The plume theory accounts for the high magmatic temperatures of komatiites (1650–1700 °C; Green et al., 1975; Herzberg, 1992), and their concentrated occurrences in the Archean,

Table 3c
Bulk rock Pb–Pb isotopic data of samples from the Nuggihalli greenstone belt, Western Dharwar craton.

Sample	Lithology	$^{206}Pb/^{204}Pb$	$\pm2\sigma$	$^{207}Pb/^{204}Pb$	$\pm2\sigma$	$^{208}Pb/^{204}Pb$	$\pm2\sigma$	r_1	r_2	μ
DHR-07-29	chromitite	14.546	0.021	14.729	0.022	34.260	0.054	0.978	0.959	7.31
DHR-07-29E	chromitite	13.515	0.014	14.480	0.016	33.291	0.040	0.975	0.948	7.55
DHR-07-29Y	chromitite	14.427	0.030	14.663	0.031	34.150	0.074	0.991	0.982	7.01
DHR-07-30A	serpentinite	13.686	0.020	14.527	0.023	33.455	0.054	0.983	0.962	7.43
DHR-07-30B	serpentinite	14.848	0.042	14.807	0.043	34.529	0.100	0.991	0.987	7.45
DHR-07-BH-1	serpentinite	17.721	0.016	15.322	0.016	36.884	0.043	0.909	0.876	8.62
DHR-07-21	serpentinite	22.777	0.020	16.268	0.016	40.167	0.043	0.971	0.942	11.86
DHR-07-24	serpentinite	18.107	0.028	15.422	0.025	38.120	0.064	0.985	0.967	8.98
DHR-07-TD-6	serpentinite	17.461	0.023	15.549	0.022	40.937	0.060	0.967	0.946	9.74
DHR-07-36	serpentinite	15.902	0.027	15.125	0.027	36.501	0.067	0.989	0.978	8.41
DHR-10-92	peridotite	25.573	0.050	16.775	0.034	43.000	0.090	0.970	0.958	13.66
DHR-10-95	peridotite	16.416	0.029	15.047	0.028	35.464	0.068	0.967	0.953	7.75
DHR-10-99	peridotite	24.514	0.030	16.699	0.023	49.491	0.071	0.935	0.918	13.42
DHR-10-129	anorthosite	14.645	0.012	14.727	0.014	34.770	0.036	0.961	0.927	7.17
DHR-10-130	anorthosite	14.528	0.019	14.652	0.020	34.543	0.050	0.978	0.955	6.82
DHR-07-26	pyroxenite	72.660	0.331	24.638	0.113	123.527	0.572	0.994	0.990	
DHR-07-35	gabbro	19.747	0.031	15.926	0.026	38.674	0.066	0.981	0.965	10.80
DHR-10-43	gabbro	15.267	0.130	14.788	0.126	34.838	0.299	0.997	0.995	7.00
DHR-10-109	gabbro	17.443	0.034	15.248	0.030	37.081	0.076	0.986	0.974	8.37
DHR-10-114	gabbro	20.584	0.018	15.896	0.016	40.229	0.044	0.938	0.908	10.57
DHR-07-33	schists	16.681	0.013	15.627	0.013	35.182	0.034	0.972	0.931	10.67
DHR-07-34	schists	15.775	0.009	15.505	0.011	33.725	0.027	0.953	0.909	11.04
DHR-07-37	schists	20.256	0.043	16.038	0.035	36.912	0.082	0.981	0.972	11.19
DHR-07-38	schists	30.913	0.043	18.821	0.027	50.051	0.076	0.976	0.956	

Table 4
Summary of crustal evolution in the Western Dharwar craton.

	Stratigraphic unit	Age
Younger Granites	Closepet–Chitradurga–Arsikere granites	2.5–2.4 Ga[e]
Younger Greenstone sequence	Bababudan–Chitradurga–Shimoga greenstone sequences containing metavolcanics and metasediments	3.0–2.5 Ga[d]
	Cumulate ultramafic-mafic suite hosting nickel sulfide and PGE mineralization, chromitite and magnetite deposits within Bababudan and Shimoga greenstone belt	2.9–2.8 Ga[c]
Older Greenstone sequence with TTG	TTG (Peninsular Gneiss)	3.4–2.9 Ga[b]
	Sargur Group metavolcanics and metasediments including sill-like layered ultramafic-mafic plutonic suite containing chromite and magnetite deposits	3.4–3.0 Ga[a] (3125 ± 120 Ma age for the sill like plutonic suite; this study)

[a] Jayananda et al. (2008), Maya et al. (2011).
[b] Jayananda and Peucat (1996);
[c] Devaraju et al. (2009) and references therein.
[d] Bhaskar Rao et al. (1992), Drury et al. (1983).
[e] Meen et al. (1992), Taylor et al. (1988).

with a subsequent decline in their occurence due to secular cooling of the Earth (Grove and Parman, 2004). However, komatiites are also thought to be generated by hydrous mantle melting at shallow depths (≈70 km) in subduction zones (e.g., Grove and Parman, 2004 and references therein).

Chromites are an effective guide to understand the tectonic setting and crust–mantle interactions in the Archean Earth (e.g., Stowe, 1994).

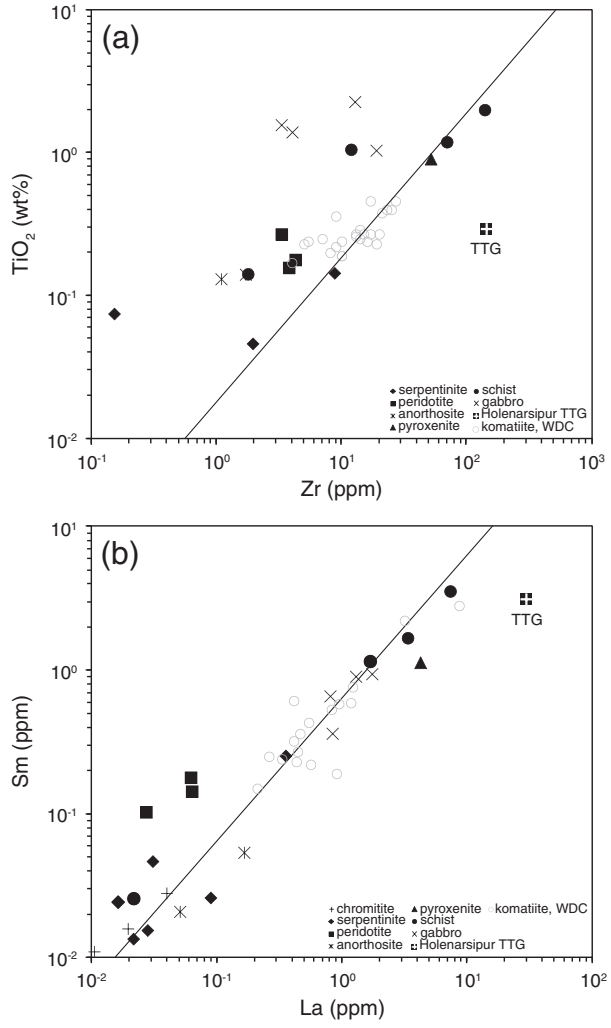

Fig. 6. Plot of (a) Zr versus TiO_2 and (b) La versus Sm for the Nuggihalli ultramafic–mafic plutonics and associated metavolcanic schists. The line illustrates the primitive mantle (McDonough and Sun, 1995) ratio. The values of Holenarsipur TTGs (Naqvi et al., 2009) have been plotted to show whether crustal contamination has affected the Nuggihalli rocks.

Study of unaltered chromites from massive chromitite in the Nuasahi–Sukinda massifs within the Archean greenstone belts (Singhbhum craton; Mondal et al., 2006), and the Archean Nuggihalli greenstone belt (Mukherjee et al., 2010) indicated a suprasubduction zone environment for the chromite deposits. The close spatial relation between the TTGs and the sill-like ultramafic–mafic, and metavolcanic schistose rocks in the Nuggihalli greenstone belt may thus be explained by the model illustrated in Fig. 7. The model shows the probable geodynamic setting in the Western Dharwar craton, where TTGs formed by melting of the subducting oceanic crust with simultaneous formation of the komatiite by hydrous melting of the depleted mantle wedge (Fig. 7). The isotopic and geochemical data of this study indicate depleted mantle as the source for the komatiite derived sill-like chromitite-bearing ultramafic–mafic complex and the metavolcanic schists in the Nuggihalli greenstone belt, and hence is consistent with the above model.

6.3. High-Mg ultramafic–mafic magmatism in the Archean and supercontinent cycles

The ε_{Nd} data of the peridotite–anorthosite–pyroxenite–gabbro from the Nuggihalli greenstone belt have been plotted against their respective ages in Fig. 8, along with data of globally occurring ultramafic–mafic rocks from greenstone belts. This figure illustrates that the mantle source of the ultramafic–mafic rocks in the Archean was depleted, and that with time the mantle has become more depleted, which is consistent with progressive extraction of the continental crust. The ε_{Nd} values of the Nuggihalli belt rocks are very similar to the range shown by the ultramafic–mafic rocks from the Yilgarn craton (Western Australia), Ivisaartoq greenstone belt (southwest Greenland), Nuasahi massif (Singhbhum craton, eastern India), and Tungurcha (Aldan craton).

The extreme range of ε_{Nd} values, shown by the ultramafic–mafic rocks from different greenstone belts in Fig. 8, indicates disturbances in the Sm–Nd system (DeWit and Ashwal, 1995). This is expected as Archean greenstone belts have a very complex history of deformation, metamorphism and later low-temperature hydrothermal alteration which are capable of resetting and modifying the isotope systematics. Despite the alteration, the relatively less altered peridotites, pyroxenite, gabbro and anorthosite depict a depleted mantle source for the Nuggihalli greenstone belt. Their average ε_{Nd} (3100 Ma) value of +2.7 is slightly higher than the depleted mantle value (+2.0) at that age (De Paolo, 1981). Jayananda et al. (2008) also obtained a range of ε_{Nd} (3352 Ma) values (+0.5 to +6.1) for the Nuggihalli komatiites that indicated a depleted mantle source for these rocks.

Fig. 8 also shows that there is an increased abundance in the occurrence of the ultramafic–mafic rocks within greenstone belts from the Early Archean till the Late Archean (i.e. from 3500 Ma to 2700 Ma), indicating major high-Mg ultramafic–mafic magmatism concentrated in the Archean (e.g., DeWit and Ashwal, 1995; Grove and Parman, 2004); this high-Mg ultramafic–mafic magmatic period spanned almost 800 Ma and may be the cause for the depleted nature

of the mantle. Such a specific and concentrated occurrence of komatiites may be associated with a supercontinent cycle.

Supercontinent cycles refer to repetitive amalgamation and break up of large blocks of the Earth's continent with a periodicity of ≈800–900 Ma (Rogers and Santosh, 2003). In the Archean, there seems to have been large hypothesized supercratons like Vaalbaara (3.5 Ga; break up ≈2.7 Ga), Superia (2.7 Ga; break up ≈2.4 Ga) and Slavia (2.6 Ga; break up ≈2.2–2.0 Ga) from which the Kaapvaal, Superior and Slave cratons were derived respectively (Bleeker, 2003). A supercontinent cycle is responsible for the formation of Large Igneous Provinces (LIPs), that represent emplacement of large volumes of mafic–ultramafic magmatism in pulses of shorter duration (1–5 Ma, maximum up to 50 Ma), in every 10–30 million years of the Earth's history (e.g., Ernst et al., 2008 and references therein). Emplacement ages of LIPs are found to correlate with periods of supercontinent break up, with the break up being initiated by mantle plume activity (Bryan and Ernst, 2008). The komatiite–tholeiite associations in Archean greenstone belts and their plutonic equivalents are also considered to be manifestations of large igneous provinces in the Archean (Bryan and Ernst, 2008).

6.4. Implications for chromite, Ni-sulfide and PGE mineralization in the Archean

Large-scale komatiitic magmatism that characterizes the Archean is not only important for the study of the crust–mantle evolution of the Earth, and the igneous processes operative during that period, but also because there is an associated boom in metallogeny observed with this type of magmatism. High-Mg ultramafic magmas such as komatiite are host to important magmatic ore mineralizations of Ni-sulfide (e.g., Arndt et al., 2005; Barnes et al., 2012; Houlé et al., 2012), while the chromite deposits occur in the plutonic ultramafic–mafic rocks of komatiitic affinity (e.g., Mondal et al., 2006; Prendergast, 2008; Rollinson, 1997). Minor PGE mineralization is observed to be associated with both Ni-sulfide and chromite deposits (e.g., Fiorentini et al., 2010; Mondal and Zhou, 2010).

An uneven temporal variation exists with respect to the distribution of metal deposits in the Earth's geological past (Barley and Groves, 1992). For example, chromite deposits are predominant in the early to mid Archean greenstone belts (3500–2900 Ma) namely, the Shurugwi greenstone belt in the Zimbabwe craton (South Africa; Rollinson, 1997; Stowe, 1987), the Tomka–Daitari–Gorumahishani–Badampahar–Jamda–Koira greenstone belts in the Singhbhum craton (eastern India; Mondal, 2009), the Nuggihalli–Krishnarajpet–Holenarsipur greenstone belts in the Western Dharwar craton (southern India; Mukherjee et al., 2010), and the Jamestown igneous complex in the Barberton greenstone belt (Kaapvaal craton, South Africa; DeWit et al., 1987). Slightly younger (≈2.7 Ga) chromite deposits within greenstone belt occur in the sill-like ultramafic complex of the Bird river sill deposit in the Superior craton, Canada (Ohnenstetter et al., 1986).

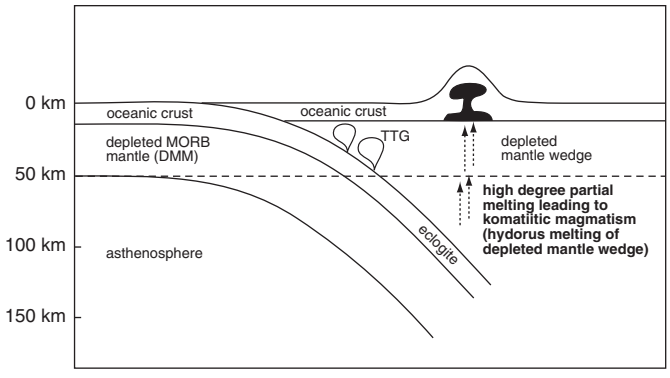

Fig. 7. Model showing the probable geodynamic setting in the Western Dharwar craton. Model illustrates the close spatial association of the TTG and the komatiitic rocks in the craton. TTG is generated by melting of the subducting slab in subduction zones while the komatiite is being generated by high degree melting of the depleted mantle wedge in a subduction zone environment.

The distribution of chromite deposits has been shown to occur over discrete periods in the Earth's history, which was considered to be a reflection of secular changes in the Earth's changing tectonic regimes and global heat flow (Stowe, 1994). The greenstone belt chromites are characterized by very high Mg-ratios (0.60–0.80) and Cr-ratios (0.68–0.78; Mondal et al., 2006; Mukherjee et al., 2010; Rollinson, 1997; Stowe, 1994), indicating high degrees of melting and derivation of the parental melts from a depleted mantle source. Similar contemporaneous early to mid Archean stratiform chromite deposits occur in high-grade gneissic terrains like the Fiskenæsset and Akilia anorthositic complexes (West Greenland; 2973 ± 28 Ma; Polat et al., 2010), and the Sittampundi complex (south India; 2935 ± 60 Ma; Bhaskar Rao et al., 1996). These high-grade terrains are also made up of dismembered ultramafic and mafic rocks, that have similar high-Mg ultramafic parentage like the ultramafic–mafic bodies within Archean greenstone belts. The initial ε_{Nd} (2973 Ma) of +3.3 ± 0.7 for ultramafic–mafic rocks of the Fiskenæsset complex indicates their derivation from a long-term depleted mantle (Polat et al., 2010). The initial ε_{Nd} (2935 Ma) of +1.85 ± 0.16 for the Sittampundi complex also indicates the same.

Archean greenstone belts also host major Ni-sulfide deposits. The Ni-sulfide deposits are concentrated mainly in the Late Archean (≈3.0 to 2.7 Ga) period of the Earth's geological history, and are related to craton–rifting processes at craton margins during regional tectonism (Begg et al., 2010; Maier and Groves, 2011). The lithosphere is thin at the margins, which facilitates transfer of melt through numerous conduits that form along the active translithospheric faults, and varying degrees of crustal interactions bring about the Ni–PGE mineralization (Begg et al., 2010). Examples of economically important Ni-sulfide deposits include the Kambalda deposit of the Yilgarn Block (Western Australia), the Abitibi greenstone belt (Superior Province, Canada), and the Bulawayan sequence of the Zimbabwe craton; no deposits occur in the older greenstone belts (≈3.5 to 3.0 Ga). Barley and Groves (1992) considered the Kambalda–type komatiite associated Ni mineralization in late Archean greenstone belts to have formed, owing to the rapid growth and stabilization of the continental crust combined with high global heat flow. Progressive accretion of volcanic–arc, marginal–basin, and related assemblages to the protocratonic nucleii during the late Archean, resulted in formation of numerous cratons that was responsible for bringing about the associated mineralization (Barley and Groves, 1992). Begg et al. (2010) also discussed that Ni-sulfide deposits occur during periods of regional compressions, continent collisions and basin inversions, and that there is a general coincidence of their occurrence with supercontinent formations. Magma plumes impinging on the sub–continental lithospheric mantle (SCLM), was considered responsible for forming large volumes of ultramafic–mafic magmas that host the Ni-sulfide deposits (Begg et al. (2010); alternatively many authors explain the magmatism to be an outcome of melting of metasomatized mantle lithosphere, by asthenospheric upwelling triggered by lithospheric delamination (Begg et al., 2010 and references therein).

Platinum group element (PGE) deposits generally occur in association with Ni-sulfide and chromite mineralization in Archean greenstone belts. PGE mineralization has been reported from the mid Archean (3.2 Ga) Nuasahi ultramafic–mafic complex in the Singhbhum craton (eastern India), where they are hosted within pegmatitic gabbroic matrix in a breccia zone (Mondal and Zhou, 2010; Mondal et al., 2001); this is an important PGE mineralized zone. PGE mineralization has also been reported from the Barberton greenstone belt (3.5 Ga Stolzburg Complex, Kaapvaal craton, South Africa; e.g., DeWit and Tredoux, 1987), Abitibi greenstone belt (2.7 Ga Alexo deposit, Superior craton, Canada; e.g., Houlé et al., 2012), Kambalda (2.7 Ga; Norseman–Wiluna greenstone belt, Yilgarn craton, Said et al., 2011), and also from the 2.7 Ga

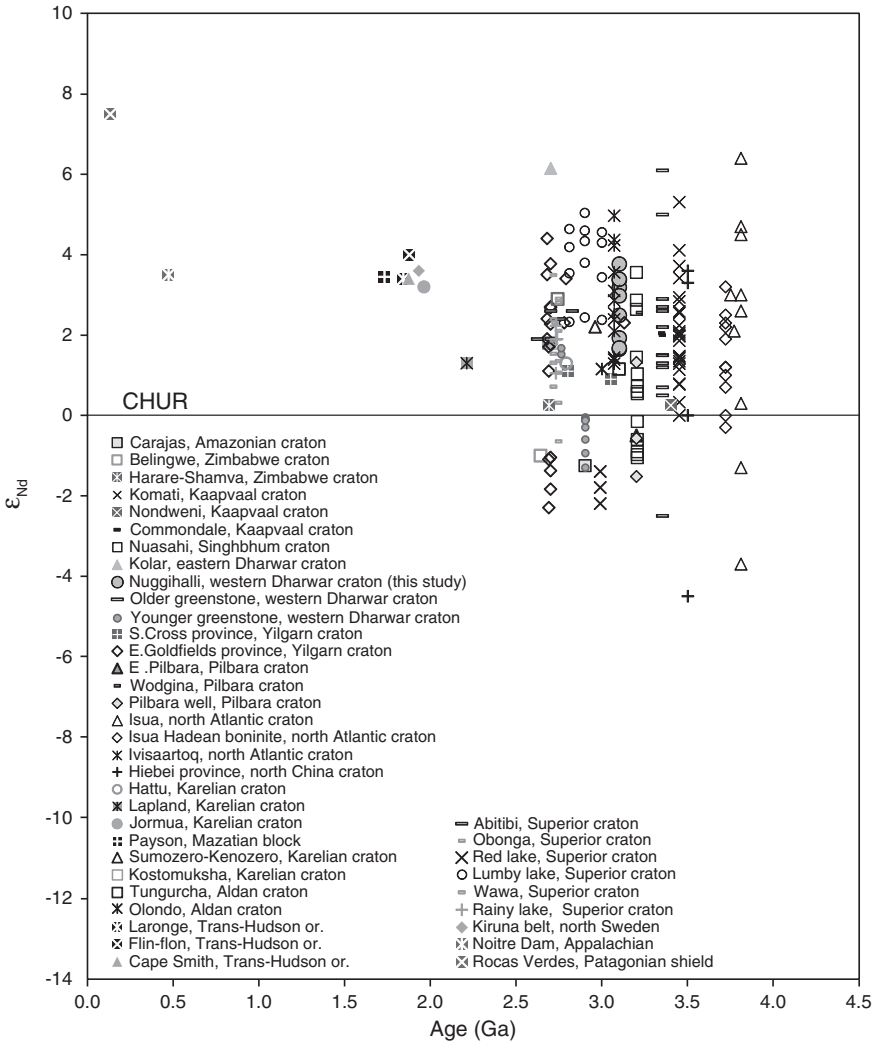

Fig. 8. Plot of age versus ε_{Nd} (initial) for ultramafic and mafic rocks like komatiites, komatiitic basalts, tholeiitic basalts, komatiitic peridotite cumulates and gabbros from different greenstone belts. The data of the Nuggihalli rocks from this study have been plotted for comparison. Other data from Chauvel et al. (1985); Shirey and Hanson (1986); Xuan et al. (1986); Shirey (1991); DeWit and Ashwal (1995); Henry et al. (1998); Tomlinson et al. (1998); Polat et al. (1999); Hollings and Wyman (1999); Bateman et al. (2001); Tomlinson et al. (2002); Augé et al. (2003); Frei and Kastbjerg Jensen (2003); Chavnac (2004); Jayananda et al. (2008); Kumar et al., 1996; Polat et al. (2008); Hoffmann et al. (2010); Van Kranendonk et al. (2010).

Ferguson Lake deposit (Yathkyed greenstone belt, Archean Churchill Province, Canadian Shield; Campos–Alvarez et al., 2012).

Thus, the observed discrete temporal distribution of different styles of metal deposits was explained by Barley and Groves (1992) to be an outcome of plate–tectonic cycles, rather than to progressive changes in the tectonic processes of the Earth. The preponderance of ore deposits of chromite from ≈3.5 to 2.7 Ga, and Ni-sulfide and PGE from ≈3.0 to 2.7 Ga are thus related to large-scale high-Mg ultramafic–mafic plutonic and volcanic events in the Earth that are connected to supercontinent cycles. There could possibly have been two supercontinents at 3.5 Ga and 2.7 Ga, with an overlap between the break up of the older hypothesized supercontinent, and the formation of the younger one; such overlaps between break up and assembly have been reported for Rodinia (Ernst et al., 2008). The suprasubduction zone setting for the 3.1 Ga chromite deposits of the Nugggihalli greenstone belt indicate that these deposits were perhaps related to the amalgamation phase of a supercontinent which culminated at 2.7 Ga.

7. Summary

A whole-rock Sm–Nd age of 3125 ± 120 Ma was obtained for the first time, for rocks belonging to the plutonic ultramafic-mafic suite with associated chromite deposits of the Nuggihalli greenstone belt in the Western Dharwar craton. The average ε_{Nd} (3100 Ma) value of +2.7 for the ultramafic plutonic rocks, and low $^{87}Sr/^{86}Sr$ values (3100 Ma) of 0.70096–0.70111 for the gabbros, indicate derivation of the parental magmas from a depleted mantle source. The REE pattern of the metavolcanic schists of the Nuggihalli greenstone belt resembles the pattern of Al-depleted komatiite. The metavolcanic schists show differentiation from komatiite to komatiitic basalt. Coherent patterns of major and trace elements, and layered nature of the ultramafic–mafic sequence indicate that the plutonic rocks are also connected by fractional crystallization. The preponderance of plutonic and volcanic ultramafic–mafic rocks of komatiitic affinity, from 3.5 Ga to 2.7 Ga in different greenstone belts is related to supercontinent cycles. Komatiites and their plutonic equivalents in the Archean greenstone belts host important metal deposits of chromite, Ni-sulfide and associated PGE mineralization. The irregular distribution of the metal deposits is also related to such supercontinent cycles. The 3.1 Ga chromite deposit of the Nugggihalli greenstone belt is perhaps related to the amalgamation stage of a supercontinent.

Supplementary data to this article can be found online at http://dx.doi.org/10.1016/j.lithos.2012.10.001.

Acknowledgements

RM wishes to acknowledge the CSIR (New Delhi) for a fellowship to conduct this research as part of her Ph.D thesis project. SKM wishes to acknowledge the Nordic Center for Earth Evolution (NordCEE), University of Copenhagen for support to conduct the analytical work. Toby Leper and Maria Jankowski are thankfully acknowledged for help during analytical work in the Isotope Geochemistry Laboratory at the IGG, University of Copenhagen. M. Lingadevaru, T. C. Devaraju and K. S. Anantha Murthy are acknowledged for guidance and support during fieldwork. SKM is grateful to the late B.P. Radhakrishna for discussion and sharing views on the Nuggihalli greenstone belt. Part of the field support came from the Geological Society of India through a field-course programme in the Nuggihalli greenstone belt led by SKM. Andrew Kerr is thankfully acknowledged for his continuous support and useful editorial comments on this article. The manuscript is highly benefitted from the constructive review by Richard Ernst, Ed Mathez, and an unidentified referee of the journal.

References

Arndt, N.T., Teixeira, N.A., White, W.M., 1989. Bizarre geochemistry of komatiites from the Crixas greenstone belt, Brazil. Contributions to Mineralogy and Petrology 101, 187–197.

Arndt, N.T., Lesher, C.M., Czamanske, G.K., 2005. Mantle-derived magmas and magmatic Ni–Cu–(PGE) deposits. Economic Geology 100th Anniversary Volume, pp. 5–23.

Arndt, N.T., Lesher, C.M., Barnes, S.J., 2008. Komatiite. Cambridge University Press, UK, p. 467.

Ashwal, L.D., 1993. Anorthosites. Springer, Verlag Berlin Heidelberg,Germany, p. 417.

Augé, T., Cocherie, A., Genna, A., Amstrong, R., Guerrot, C., Mukherjee, M.M., Patra, R.N., 2003. Age of the Baula PGE mineralization (Orissa, India) and its implications concerning the Singhbhum Archean Nucleus. Precambrian Research 121, 85–101.

Barley, M.E., Groves, D.I., 1992. Supercontinent cycles and the distribution of metal deposits through time. Geology 20, 291–294.

Barnes, S.J., 2006. Komatiites: petrology, volcanology, metamorphism, and geochemistry. Society of Economic Geologists Special Publication 13, 13–49.

Barnes, S.J., Gole, M.J., Hill, R.E.T., 1988. The Agnew nickel deposit, Western Australia: Part I. Structure and stratigraphy. Economic Geology 83, 524–536.

Barnes, S.J., Fiorentini, M.L., Fardon, M.C., 2012. Platinum group element and nickel sulphide ore tenors of the Mount Keith nickel deposit, Yilgarn craton, Australia. Mineralium Deposita 47, 129–150.

Bateman, R., Costa, S., Swe, T., Lambert, D., 2001. Archaean mafic magmatism in the Kalgoorlie area of the Yilgarn craton, Western Australia: a geochemical and Nd isotopic study of the petrogenetic and tectonic evolution of a greenstone belt. Precambrian Research 108, 75–112.

Beckinsale, R.D., Drury, S.A., Holt, R.W., 1980. 3360-Myr old gneisses from the South Indian craton. Nature 283, 469–470.

Beckinsale, R.D., Reeves–Smith, G., Gale, N.H., Holt, R.W., Thompson, B., 1982. Rb–Sr and Pb–Pb whole rock isochron ages and REE data for Archean gneisses and granites, Karnataka State, South India. Indo–US Workshop on Precambrians of South India, National Geophysical Research Institute, Hyderabad, India: Abstracts of the papers, pp. 35–36.

Begg, G.C., Hronsky, J.A.M., Arndt, N.T., Griffin, W.L., O'Reilly, S.Y., Hayward, N., 2010. Lithospheric, cratonic, and geodynamic setting of Ni–Cu–PGE sulfide deposits. Economic Geology 105, 1057–1070.

Bell, K., Blenkinsop, J., Cole, T.J.S., Menagh, D.P., 1982. Evidence from Sr isotopes for long lived heterogeneities in the upper mantle. Nature 298, 251–253.

Bhaskar Rao, Y.J., Sivaraman, T.V., Pantulu, C.V.C., Gopalan, K., Naqvi, S.M., 1992. Rb–Sr ages of late Archean metavolcanics and granites, Dharwar craton, south India and evidence for early Proterozoic thermotectonic event(s). Precambrian Research 59, 145–170.

Bhaskar Rao, Y.J., Chetty, T.R.K., Janardhan, A.S., Gopalan, K., 1996. Sm–Nd and Rb–Sr ages and P–T history of the Archean Sittampundi and Bhavani layered meta–anorthosite complexes in Cauvery shear zone, South India: evidence for Neoproterozoic reworking of Archean crust. Contributions to Mineralogy and Petrology 125, 237–250.

Bidyananda, M., Mitra, S., 2005. Chromitites from komatiitic affinity from the Archean Nuggihalli greenstone belt in South India. Mineralogy and Petrology 84, 169–187.

Bidyananda, M., Deomurari, M.P., Goswami, J.N., 2003. ^{207}Pb–^{206}Pb ages of zircon from the Nuggihalli schist belt, Dharwar craton, southern India. Current Science 85, 1482–1485.

Bleeker, W., 2003. The late Archean record: a puzzle in ca. 35 pieces. Lithos 91, 99–134.

Bryan, S.E., Ernst, R.E., 2008. Revised definition of large igneous provinces (LIPs). Earth-Science Reviews 86, 175–202.

Campbell, I.H., Griffiths, R.W., Hill, R.I., 1989. Melting in an Archean mantle plume: head its basalts and tail its komatiites. Nature 339, 697–699.

Campos–Alvarez, N.O., Samson, I.M., Fryer, B.J., 2012. The roles of magmatic and hydrothermal processes in PGE mineralization, Ferguson Lake deposit, Nunavut, Canada. Mineralium Deposita 47, 441–465.

Chauvel, C., Dupré, B., Jenner, G.A., 1985. The Sm–Nd age of Kambalda volcanics is 500 Ma too old. Earth and Planetary Science Letters 74, 315–324.

Chavnac, V., 2004. A geochemical and Nd isotopic study of Barberton komatiites (South Africa): implication for the Archean mantle. Lithos 75, 253–281.

De Paolo, D.J., 1981. Neodymium isotopes in Colarado Front Range and crust–mantle evolution in Proterozoic. Nature 291, 193–196.

Devaraju, T.C., Viljoen, R.P., Sawkar, R.H., Sudhakara, T.L., 2009. Mafic and ultramafic magmatism and associated mineralization in the Dharwar craton, southern India. Journal of Geological Society of India 73, 73–100.

DeWit, M.J., Ashwal, L.D., 1995. Greenstone belts: what are they? South African Journal of Geology 98, 505–520.

DeWit, M.J., Tredoux, M., 1987. In: Prichard, H.M., Potts, P.J., Bowles, J.F.W., Cribb, S.J. (Eds.), PGE in the 3.5 Ga Jamestown Ophiolite Complex, Barberton greenstone belt, with implications for PGE distribution in simatic lithosphere. Proceedings of the symposium GeoPlatinum, 87. Elsevier, London and New York, pp. 319–341.

DeWit, M.J., Hart, R.A., Hart, R.J., 1987. The Jamestown ophiolite complex, Barberton mountain belt: a section through 3.5 Ga oceanic crust. Journal of African Earth Sciences 6, 681–730.

Dey, S., 2012. Evolution of Archaean crust in the Dharwar craton: the Nd isotope record. Precambrian Research http://dx.doi.org/10.1016/j.precamres.2012.05.005.

Donaldson, M.J., Lesher, C.M., Groves, D.I., Gresham, J.J., 1986. Comparison of Archaean dunites and komatiites associated with nickel mineralization in Western Australia: implications for dunite genesis. Mineralium Deposita 21, 296–305.

Drury, A.S., Holt, R.W., Van Calsteren, P.C., Beckinsale, R.D., 1983. Sm–Nd and Rb–Sr ages for Archean rocks in western Karnataka, South India. Journal of Geological Society of India 24, 454–459.

Drury, S.A., Van Calstren, P.C., Reeves–Smith, G.J., 1987. Sm–Nd isotopic data from Archaean metavolcanic rocks at Holenarsipur, South India. Journal of Geology 95, 837–843.

Ernst, R.E., Wingate, M.T.D., Buchan, K.L., Li, Z.X., 2008. Global record of 1600–700 Ma Large Igneous Provinces (LIPs): implications for the reconstruction of the proposed Nuna (Columbia) and Rodinia supercontinents. Precambrian Research 160, 159–178.

Fan, J., Kerrich, R., 1997. Geochemical characteristics of aluminium depleted and undepleted komatiites and HREE-enriched low-Ti tholeiites, western Abitibi greenstone belt: a heterogeneous mantle plume-convergent margin environment. Geochimica et Cosmochimica Acta 61, 4723–4744.

Fiorentini, M.L., Barnes, S.J., Lesher, C.M., Heggie, G.J., Keays, R.R., Burnham, O.M., 2010. Platinum group element geochemistry of mineralized and nonmineralized komatiites and basalts. Economic Geology 105, 795–823.

Frei, R., Kastbjerg Jensen, B., 2003. Re–Os, Sm–Nd isotope– and REE systematics on komatiites and pillow basalts from the Earth's oldest oceanic crustal fragments (Isua Supracrustal Belt, W Greenland). Chemical Geology 196, 163–191.

Ghiorso, M.S., Sack, R.O., 1995. Chemical mass transfer in magmatic processes. IV. A revised and internally consistent thermodynamic model for the interpolation and extrapolation of liquid–solid equilibria in magmatic systems at elevated temperatures and pressures. Contributions to Mineralogy and Petrology 119, 197–212.

Green, D.H., Nicholls, I.A., Viljoen, M., Viljoen, R., 1975. Experimental demonstration of the existence of peridotitic liquids in earliest Archean magmatism. Geology 3, 11–14.

Grove, T.L., Parman, S.W., 2004. Thermal evolution of the earth as recorded by komatiites. Earth and Planetary Science Letters 219, 173–187.

Henry, P., Stevenson, R.K., Gariépy, C., 1998. Late Archean mantle composition and crustal growth in the Western Superior Province of Canada: neodymium and lead isotopic evidence from the Wawa, Quetico, and Wabigoon subprovinces. Geochimica et Cosmochimica Acta 62, 143–157.

Herzberg, C.T., 1992. Depth and degree of melting of komatiites at high pressures. Journal of Geophysical Research 97, 4521–4540.

Herzberg, C., 1995. Generation of plume magmas through time—an experimental perspective. Chemical Geology 126, 1–16.

Hill, R.E.T., Barnes, S.J., Gole, M.J., Dowling, S.E., 1995. The volcanology of komatiites as deduced from field relationships in the Norseman–Wiluna greenstine belt, Western Australia. Lithos 34, 159–188.

Hoffmann, J.E., Münker, C., Polat, A., König, S., Mezger, K., Rosing, M.T., 2010. Highly depleted Hadean mantle reservoirs in the sources of early Archean arc-like rocks, Isua supracrustal belt, southern West Greenland. Geochimica et Cosmochimica Acta 74, 7236–7260.

Hollings, P., Wyman, D., 1999. Trace element and Sm–Nd systematics of volcanic and intrusive rocks from the 3 Ga Lumby Lake Greenstone belt, Superior Province: evidence for Archean plume–arc interaction. Lithos 46, 189–213.

Horowitz, E.P., Chiarizia, R., Dietz, M.L., 1992. A novel strontium-selective extraction chromatographic resin. Solvent Extraction and Ion Exchange 10, 313–336.

Houlé, M.G., Lesher, C.M., Davis, P.C., 2012. Thermomechanical erosion at the Alexo Mine, Abitibi greenstone belt, Ontario: implications for the genesis of komatiite–associated Ni– Cu–(PGE) mineralization. Mineralium Deposita 47, 105–128.

Jafri, S.H., Khan, N., Ahmed, S.M., Saxena, R., 1983. Geology and geochemistry ofNuggihalli schist belt, Dharwar craton, Karnataka, India. In: Naqvi, S.M., Rogers, J.J.W. (Eds.), Precambrian of South India: Memoirs Geological Society of India, 4, pp. 110–120.

Jayananda, M., Peucat, J.-J., 1996. In: Santosh, M., Yoshida, M. (Eds.), Geochronological framework of Southern India: the Archaean and Proterozoic terrains of Southern India within East Gondwana: Gondowana Research Group Memoir, 3, pp. 53–75.

Jayananda, M., Kano, T., Peucat, J.J., Channabasappa, S., 2008. 3.35 Ga komatiite volcanism in the Western Dharwar craton, southern India: constraints from Nd isotopes and whole-rock geochemistry. Precambrian Research 162, 160–179.

Kamenetsky, V.S., Crawford, A.J., Meffre, S., 2001. Factors controlling chemistry of magmatic spinel: an empirical study of associated olivine, Cr-spinel and melt inclusions from primitive rocks. Journal of Petrology 42, 655–671.

Kerrich, R., Wyman, D., Fan, J., Bleeker, W., 1998. Boninite series: low Ti–tholeiite associations from the 2.7 Ga Abitibi greenstone belt. Earth and Planetary Science Letters 164, 303–316.

Kumar, A., Bhaskar Rao, Y.J., Sivaraman, T.V., Gopalan, K., 1996. Sm–Nd ages of Archean metavolcanics of the Dharwar craton, South India. Precambrian Research 80, 205–216.
Leelananadam, C., Burke, K., Ashwal, L.D., Webb, S.J., 2006. Proterozoic mountain building in Peninsular India: an analysis based primarily on alkaline rock distribution. Geological Magazine 143, 1–18.
Lesher, C.M., Groves, D.I., 1986. Controls on the formation of komatiite-associated nickel–copper sulfide deposits. In: Friedrich, G.H. (Ed.), Geology and Metallogeny of Copper Deposits. Springer, Berlin, pp. 63–90.
Ludwig, K.R., 2008. User's Manual for ISOPLOT 3.6. A Geochronological Tool Kit for Microsoft Excel. Berkely Geochronology Centre Special Publication No. 4. Berkely, CA, USA.
Maier, W.D., Groves, D.I., 2011. Temporal and spatial controls on the formation of magmatic PGE and Ni–Cu deposits. Mineralium Deposita 46, 639–657.
Maurel, C., Maurel, P., 1982. Etude expérimentale de la solubilité du chrome dans les bains silicatés basiques et sa distribution entre liquide et minéraux coexistants: conditions d'existence du spinelle chromifére. Bulletin de Mineralogie 105, 197–202.
Maya, J.M., Bhutani, R., Balakrishnan, S., 2011. $^{146,147}Sm$–$^{142,143}Nd$ studies of komatiites from Western Dharwar craton, India: implications for depleted mantle evolution in Early Archean. Mineralogical Magazine, 1430. Goldschmidt Abstract, Prague.
McDonough, W.F., Sun, S.-S., 1995. The composition of the Earth. Chemical Geology 120, 223–253.
Meen, J.K., Rogers, J.J.W., Fullagar, P.D., 1992. Lead isotopic composition in the Western Dharwar craton, southern India: evidence for distinct middle Archean terrains in a late Archaean craton. Geochimica et Cosmochimica Acta 56, 2455–2470.
Mondal, S.K., 2000. Study of chromite, sulfide, and noble metal mineralization in the Precambrian Nuasahi ultramafic–mafic complex, Keonjhar district, Orissa, India. Unpublished PhD Thesis. Jadavpur University, Calcutta, India, p. 193.
Mondal, S.K., 2009. Chromite and PGE deposits of Mesoarchean ultramafic–mafic suites within the greenstone belts of the Singhbhum craton, India: implications for mantle heterogeneity and tectonic setting. Journal of Geological Society of India 73, 36–51.
Mondal, S.K., Zhou, M.F., 2010. Enrichment of PGE through interaction of evolved boninitic magmas with early formed cumulates in a gabbro–breccia zone of the Mesoarchean Nuasahi massif (eastern India). Mineralium Deposita 45, 69–91.
Mondal, S.K., Baidya, T.K., Rao, K.N.G., Glascock, M.D., 2001. PGE and Ag mineralization in a breccia zone of the Precambrian Nuasahi ultramafic–mafic Complex, Orissa, India. The Canadian Mineralogist 39, 979–996.
Mondal, S.K., Ripley, E.M., Li, C., Frei, R., 2006. The genesis of Archean chromitites from the Nuasahi and Sukinda massifs in the Singhbhum craton, India. Precambrian Research 148, 45–66.
Mondal, S.K., Frei, R., Ripley, E.M., 2007. Os isotope systematics of Mesoarchaean chromitite–PGE deposits in the Singhbhum craton (India): implications for the evolution of lithospheric mantle. Chemical Geology 244, 391–408.
Monrad, J.R., 1983. Evolution of sialic terranes in the vicinity of the Holenarsipur beltHassan District. In: Naqvi, S.M., Rogers, J.J.W. (Eds.), Precambrian ofSouth India: Geological Society of India Memoir, 4, pp. 343–364.
Moyen, J.-F., 2011. The composite Archaean grey gneisses: petrological significance, and evidence for a non-unique tectonic setting for Archaean crustal growth. Lithos 123, 21–36.
Moyen, J-F., Martin, H., 2012. Forty years of TTG research. Lithos 148, 312–336.
Mukherjee, R., Mondal, S.K., Rosing, M.T., Frei, R., 2010. Compositional variations in the Mesoarchean chromites of the Nuggihalli schist belt, Western Dharwar craton (India): potential parental melts and implications for tectonic setting. Contributions to Mineralogy and Petrology 160, 865–885.
Mungall, J.E., Staff, N.G., 2008. Formation of massive chromitite by assimilation of iron formation in the Blackbird deposit, Ontario, Canada. Eos Transaction AGU 89 (53) (Fall Meeting Supplement, Abstract V11A–2014).
Murthy, N.G.K., 1987. Mafic dyke swarms of the Indian shield, Mafic swarms. Geological Association of Canada special paper 34, 393–400.
Naldrett, A.J., Turner, A.R., 1977. The geology and petrogenesis of a greenstone belt and related nickel-sulfide mineralization at Yakabindie, Western Australia. Precambrian Research 5, 43–103.
Naqvi, S.M., Hussain, S.M., 1979. Geochemistry of meta-anorthosites from a greenstone belt in Karnataka, India. Canadian Journal of Earth Sciences 16, 1254–1264.
Naqvi, S.M., Ram Mohan, M., Rana Prathap, J.G., Srinivasa Sarma, D., 2009. Adakite–TTG connection and fate of Mesoarchaean basaltic crust of Holenarsipur Nucleus, Dharwar craton, India. Journal of Asian Earth Sciences 35, 416–434.
Nutman, A.P., Chadwick, B., Ramakrishnan, M., Viswanatha, M.N., 1992. SHRIMP U–Pb ages of detrital zircon in Sargur supracrustal rocks in western Karnataka, southern India. Journal of Geological Society of India 39, 367–374.
Ohnenstetter, D., Watkinson, D.H., Jones, P.C., Talkington, R., 1986. Cryptic Compositional Variation in Laurite and Enclosing Chromite from the Bird River Sill, Manitoba. Economic Geology 81, 1159–1168.
Pearce, J.A., Norry, M.J., 1979. Petrogenetic implications of Ti, Zr, Y, and Nb variations in volcanic rocks. Contributions to Mineralogy and Petrology 69, 33–47.
Peucat, J.-J., Bouhallier, H., Fanning, C.M., Jayananda, M., 1995. Age of Holenarsipur schist belt, relationships with the surrounding gneisses (Karnataka, south India). Journal of Geology 103, 701–710.
Polat, A., Kerrich, R., Wyman, D.A., 1999. Geochemical diversity in oceanic komatiites and basalts from the late Archean Wawa greenstone belts, Superior Province, Canada: trace element and Nd Isotope evidence for a heterogeneous mantle. Precambrian Research 94, 139–173.
Polat, A., Frei, R., Appel, P.W.U., Dilek, Y., Fryer, B., Ordóñez-Calderón, J.C., Yang, Z., 2008. The origin and compositions of Mesoarchean oceanic crust: Evidence from the 3075 Ma Ivisaartoq greenstone belt, SW Greenland. Lithos 100, 293–321.
Polat, A., Frei, R., Scherstén, A., Appel, P.W.U., 2010. New age (ca. 2970 Ma), mantle source composition and geodynamic constraints on the Archean Fiskenæsset anorthosite complex, SW Greenland. Chemical Geology 277, 1–20.
Prendergast, M.D., 2008. Archean komatiitic sill-hosted chromite deposits in the Zimbabwe craton. Economic Geology 103, 981–1004.
Radhakrishna, B.P., Naqvi, S.M., 1986. Precambrian continental crust of India and its evolution. Journal of Geology 94, 145–166.
Radhakrishnan, B.P., Pandit, S.A., Prabhakar, K.T., 1973. Copper mineralization in the Ultrabasic Complex of Nuggihalli, Hassan District, Mysore State. Journal of Geological Society of India 14, 302–312.
Ramakrishnan, M., Venkatadasu, S.P., Kroner, A., 1994. Middle Archaean age of Sargur Group by single grain zircon dating and geochemical evidence for the clastic origin of metaquartzite from J.C. Pura Greenstone belt, Karnataka. Journal of Geological Society of India 44, 605–616.
Rogers, J.J.W., Santosh, M., 2003. Supercontinents in Earth history. Gondowana Research 6, 357–368.
Rollinson, H., 1997. The Archaean komatiite-related Inyala chromitite, Southern Zimbabwe. Economic Geology 92, 98–107.
Said, N., Kerrich, R., Maier, W.D., Campbell, M., 2011. Behaviour of Ni–PGE–Au–Cu in mafic–ultramafic volcanic suites of the 2.7 Ga Kambalda sequence, Kalgoorlie terrane, Yilgarn craton. Geochimica et Cosmochimica Acta 75, 2882–2910.
Shirey, S.B., 1991. The Rb–Sr, Sm–Nd and Re–Os isotopic systems: a summary and comparison of their applications to the cosmochronolgy and geochronology of igneous rocks. In: Heaman, L., Ludden, J.N. (Eds.), Applications of radiogenic isotope systems to problems in geology: Mineralogical Association of Canada, 19, pp. 103–162.
Shirey, S.B., Hanson, G., 1986. Mantle heterogeneity and crustal recycling in Archean granite–greenstone belts: evidence from Nd isotopes and trace elements in the Rainy Lake area, Superior Province, Ontario, Canada. Geochimica et Cosmochimica Acta 50, 2631–2651.
Stacey, J.S., Kramers, J.D., 1975. Approximation of terrestrial lead isotope evolution by a two-stage model. Earth and Planetary Science Letters 26, 207–221.
Stowe, C.W., 1987. Chromite deposits of the Shurugwi greenstone belt, Zimbabwe. In: Stowe, C.W. (Ed.), Evolution of chromium ore fields. Van Nostrand Reinhold, New York, pp. 71–88.
Stowe, C.W., 1994. Compositions and tectonic settings of chromite deposits though time. Economic Geology 89, 528–546.
Stroh, P.T., Monrad, J.R., Fullagar, P.D., Naqvi, S.M., Hussain, S.M., Rogers, J.J.W., 1983. 3,000-m.y.-old Halekote Trondhjemite. In: Naqvi, S.M., Rogers, J.J.W. (Eds.), PrecambrianSouth India Naqvi: Geological Society of India Memoir, 4, pp. 365–376.
Sun, S.S., Nesbitt, R.W., 1978. Petrogenesis of Archaean ultrabasic and basic volcanics. Evidence from rare earth elements. Contributions to Mineralogy and Petrology 65, 301–325.
Swami Nath, J., Ramakrishnan, M., 1981. Early Precambrian supracrustals of Southern Karnataka Mem. Geological Survey of India 112, 363.
Taylor, P.N., Chadwick, B., Moorbath, S., Ramakrishnan, M., Viswanatha, M.N., 1984. Petrography, chemistry and isotopic ages of peninsular gneisses, Dharwar acid volcanic rocks and the Chitradurga granite with special reference to the late Archaean evolution of the Karnataka craton. Precambrian Research 23, 349–375.
Taylor, P.N., Chadwick, B., Friend, C.R.L., Ramakrishnan, M., Moorbath, S., Viswanatha, M.N., 1988. New age data on the geological evolution of Southern India. Workshop on the deep continental crust of South India, January 1988. Journal of Geological Society of India 31, 155–158.
Todt, W., Cliff, R.A., Hanser, A., Hofmann, A.W., 1993. Re calibration of NBS lead standards using a 202Pb + 205Pb double spike. Terra Abstracts 5 (Suppl. 1), 396.
Tomlinson, K.Y., Stevenson, R.K., Hughes, D.J., Hall, R.P., Thurston, P.C., Henry, P., 1998. The Red Lake greenstone belt, Superior Province: evidence of plume-related magmatism at 3 Ga and evidence of an older enriched source. Precambrian Research 89, 59–76.
Tomlinson, K.Y., Davis, D.W., Percival, J.A., Hughes, D.J., Thurston, P.C., 2002. Mafic to felsic magmatism and crustal recycling in the Obonga Lake greenstone belt, western Superior Province: evidence from geochemistry, Nd isotopes and U–Pb geochronology. Precambrian Research 114, 295–325.
Van Kranendonk, M.J., Smithies, H.R., Hickman, A.H., Wingate, M.T.D., 2010. Evidence for Mesoarchean (3.2 Ga) rifting of the Pilbara craton: the missing link in an early Precambrian Wilson cycle. Precambrian Research 177, 145–161.
Xuan, H., Ziwei, B., DePaolo, D.J., 1986. Sm–Nd isotope study of early Archean rocks, Qianan, Hebei Province, China. Geochimica et Cosmochimica Acta 50, 625–631.